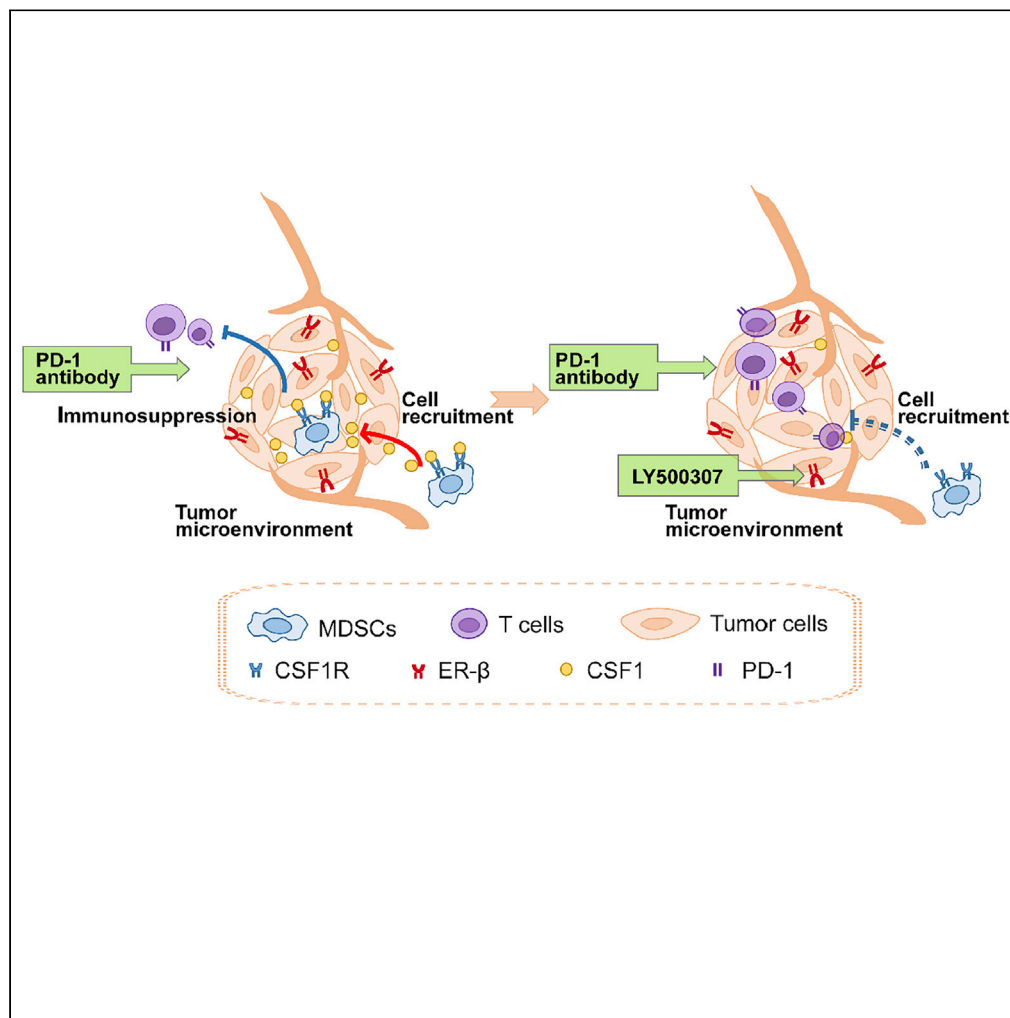


Article

Pharmacological Activation of Estrogen Receptor Beta Overcomes Tumor Resistance to Immune Checkpoint Blockade Therapy



Shuang Huang,
Nianxin Zhou,
Linjie Zhao, ...,
Hongbo Hu, Jan-Åke Gustafsson,
Shengtao Zhou

jgustafsson@uh.edu (J.-Å.G.)
taotaovip2005@163.com,
shengtaozhou@scu.edu.cn
(S.Z.)

HIGHLIGHTS

ERβ activation overcomes ICB resistance in tumors

ERβ activation and ICB therapy reduces MDSC infiltration and increases cytotoxic T cells

CSF1/CSF1R axis is suppressed in combined therapy of ERβ activation and ICB therapy



Article

Pharmacological Activation of Estrogen Receptor Beta Overcomes Tumor Resistance to Immune Checkpoint Blockade Therapy

Shuang Huang,^{1,11} Nianxin Zhou,^{1,11} Linjie Zhao,² Ryan C. Gimple,^{2,3} Young Ha Ahn,⁴ Peidong Zhang,¹ Wei Wang,¹ Bin Shao,⁵ Jingyun Yang,¹ Qian Zhang,¹ Sai Zhao,⁶ Xuehan Jiang,⁷ Zhiwei Chen,¹ Yangfan Zeng,¹ Hongbo Hu,⁸ Jan-Åke Gustafsson,^{9,10,*} and Shengtao Zhou^{1,12,*}

SUMMARY

The emerging immune checkpoint blockade (ICB) therapy has ushered the cancer therapeutics field into an era of immunotherapy. Although ICB treatment provides remarkable clinical responses in a subset of patients with cancer, this regimen fails to extend survival in a large proportion of patients. Here, we found that a combined treatment of estrogen receptor beta (ER β) agonist and PD-1 antibody treatment improved therapeutic efficacy in mouse tumor models, compared with monotherapies, by reducing infiltration of myeloid-derived suppressor cells (MDSCs) and increasing CD8⁺ T cells in tumors. Mechanistically, LY500307 treatment reduced tumor-derived CSF1 and decreased infiltration of CSF1R⁺ MDSCs in the tumor bed. CSF1 released by tumor cells induced CSF1R⁺ MDSC chemotaxis *in vitro* and blockade of CSF1R demonstrated similar therapeutic effects as ER β activation *in vivo*. Collectively, our study proved combined treatment of ER β agonist and PD-1 antibody reduced MDSC infiltration in the tumor and enhanced tumor response to ICB therapy.

INTRODUCTION

The human immune system is responsible for the clearance of pathogens and transformed cells. This usually requires functionally redundant counterbalance mechanisms to ensure safety and avoid overreaction (Wykes and Lewin, 2018). In the tumor microenvironment, cancer cells often hijack this counterbalance system to avoid self-destruction and mediate immune evasion. Immune checkpoint molecules are inhibitory receptors expressed on immune cells that elicit immunosuppressive signaling pathways, which constitute an important part of this system. These molecules play critical roles in sustaining self-tolerance and for modulating the length and magnitude of effector immune responses (Fritz and Lenardo, 2019; Pauken et al., 2019; Sanmamed and Chen, 2018). Recently, the checkpoints guarded by the programmed cell death-1 (PD-1) and cytotoxic T-lymphocyte-associated antigen-4 (CTLA-4) receptors have been intensively explored owing to the availability of antibodies that can inhibit their function (Gordon et al., 2017; Minn and Wherry, 2016; Patel and Minn, 2018). With the remarkable therapeutic effects of anti-CTLA-4, anti-PD-1, and anti-PD-L1 monoclonal antibodies in preclinical models and clinical trials, the US Food and Drug Administration has approved their clinical use for the treatment of a variety of cancers.

Although immune checkpoint blockade (ICB) therapy has greatly improved objective response rates, time to progression, and overall survival in some patients with cancer, the majority of patients still fail to respond to ICB therapy. The reported molecular mechanisms include a variety of factors within the tumor microenvironment, for instance, the infiltration of immunosuppressive immune cells including Treg cells, myeloid-derived suppressor cells (MDSCs), and indole 2,3-dioxygenase (IDO) activity. Furthermore, tumor-cell-autonomous factors including mutational load, oncogenic signaling pathways, expression of PD-L1, and down-regulation of major histocompatibility complex (MHC) class I likely contribute as well (Conway et al., 2018; Keenan et al., 2019; Pitt et al., 2016). Apart from these tumor-intrinsic influences, other host-related and environmental factors affecting immune system function could also be involved in the development of checkpoint blockade therapy resistance, like the heterogeneity of gut microbiota (Gopalakrishnan et al., 2018; Routy et al., 2018). Thus, it is important to find ways to improve the response rate of patients with cancer to ICB therapy.

¹Department of Obstetrics and Gynecology, Key Laboratory of Birth Defects and Related Diseases of Women and Children of MOE and State Key Laboratory of Biotherapy, West China Second Hospital, Sichuan University and Collaborative Innovation Center, Chengdu, P. R. China

²Division of Regenerative Medicine, Department of Medicine, University of California, San Diego, CA, USA

³Department of Pathology, Case Western Reserve University, Cleveland, OH, USA

⁴Immunotherapy Convergence Research Center, Korea Research Institute of Bioscience and Biotechnology (KRIBB), 125 Gwahak-ro, Yuseong-gu, Daejeon, Republic of Korea

⁵State Key Laboratory of Oral Diseases, National Clinical Research Center for Oral Diseases, West China Hospital of Stomatology, Sichuan University, Chengdu, P. R. China

⁶Department of Biotherapy, State Key Laboratory of Biotherapy and Cancer Center, West China Hospital, and West China School of Basic Medical Sciences & Forensic Medicine, Sichuan University, and Collaborative Innovation Center for Biotherapy, Chengdu, P. R. China

⁷College of Life Science, Sichuan University, Chengdu, P. R. China

⁸Department of Rheumatology and Immunology, State Key Laboratory of Biotherapy, West China Hospital, Sichuan University, and Collaborative

Continued



Estrogenic actions are mediated mainly through two distinct estrogen receptor (ER) subtypes: ER α and ER β . In contrast to the tumor-promoting role of ER α in hormone-responsive cancer, ER β is reported to be tumor suppressive and has a major role in the immune system. In this study, we aim to evaluate whether pharmacological activation of ER β could exert therapeutic effects for ICB therapy-resistant tumors and the possible mechanisms of effects.

RESULTS

Combination of ER β Activation and ICB Therapy Improves Therapeutic Efficacy in TNBC and Colorectal Cancers

Previous evidence has proved expression of ER β in triple-negative breast cancer (TNBC) (Reese et al., 2018; Zhao et al., 2018) and colorectal cancer tissues (Ibrahim et al., 2019; Williams et al., 2016) and its potential role as therapeutic targets for these tumors. In addition, TNBC and colorectal cancer have demonstrated resistance to ICB therapy (Kim et al., 2014). In an effort to explore whether ER β activation could overcome ICB resistance in TNBC and colorectal cancers, we first evaluated the specificity of LY500307 for ER β activation. Based upon the results demonstrated in a previous report (Reese et al., 2018), we examined whether LY500307 could induce increased expression of ER β target genes. It was demonstrated that LY500307 could up-regulate the expression of CXCL14, KRT17, IGFBP4, KRT13, and Ankrd33, which are known ER β target genes (Figure S1A). We further analyzed the *bona fide* targets of ER β by analyzing the publicly available Chip sequencing dataset GSE108979. Principle component analysis (PCA) demonstrated that each replicate consistently showed altered DNA binding profiles (Figure S1B). The differential ER β -binding regions on DNA were demonstrated (Figure S1C). After comparing genes that are both up-regulated after ER β activation identified by RNA sequencing and are found to be regulated by ER β identified by Chip sequencing, we found 111 overlapping genes, which are *bona fide* transcriptional targets of ER β (Figure S1D). Among them, the peak view of IGFBP4 as a representative ER β -target gene was illustrated (Figure S1E). These data suggested that LY500307 specifically activates ER β .

Next, we established a BALB/c mouse model bearing subcutaneous 4T1 and CT26 tumors for the evaluation of therapeutic effects of combined PD-1 antibody and a selective ER β agonist, LY500307, therapies as well as PD-1 antibody or LY500307 monotherapies (Figure 1A). We observed that, although either PD-1 antibody or LY500307 monotherapies had minimal impact on TNBC tumor growth, the combination of PD-1 antibody and LY500307 showed synergistic efficacy in targeting TNBC growth (Figure 1B). No obvious effects on the body weight of those mice were observed in each treatment group (Figure 1C). At indicated time point, the volume and weight of the tumors in the combined treatment group were significantly reduced compared with monotherapy groups and control (Figures 1D and 1E). Similarly, in a corroborating study with CT26 model, combined therapy of PD-1 antibody and LY500307 also showed synergistic efficacy in targeting colorectal cancer growth (Figure 1F), as revealed by tumor volume and tumor weight at indicated time point (Figures 1H and 1I). Mouse body weight was unaffected in each group in CT26 models as well (Figure 1G). In an orthotopic breast cancer model, we also observed that combined treatment with PD-1 antibody and LY500307 showed significantly better therapeutic efficacy compared with each monotherapy or control (Figure 1J), in terms of tumor volume (Figure 1L) and tumor weight (Figure 1M). No significant difference was observed in the body weight of mice in each group as well (Figure 1K). Moreover, we observed a significantly increased level of apoptosis and diminished proliferation rate of tumors in the combined treatment group compared with each monotherapy group and control, as revealed by immunohistochemistry analysis of cleaved caspase 3 and Ki-67 staining, respectively (Figures S2A and S2B).

In addition, we further validated our findings by genetic approaches. We first constructed ER β -overexpressing plasmid and obtained an ER β -overexpressing 4T1 cell line (Figures S3A and S3B). We found that, in the orthotopic 4T1 model, the group of 4T1 cells overexpressing ER β treated together with PD-1 antibody group, similar to that of combined treatment group of LY500307 and PD-1 antibody, grew much slower compared with other groups (Figure S3E). No obvious effects on the body weight of those mice were observed in each treatment group (Figure S3F). At indicated time point, the volume and weight of the tumors in the group of 4T1 cells overexpressing ER β treated together with PD-1 antibody group, similar to those of combined treatment group of LY500307 and PD-1 antibody, were significantly reduced compared with other groups (Figures S3G and S3H). By contrast, we also constructed ER β knockdown 4T1 cell line by transfecting shER β plasmids (Figures S3C and S3D). It was demonstrated that, after ER β knockdown, the therapeutic efficacy of combined treatment with LY500307 and PD-1 was abolished (Figures S3I, S3K, and S3L). No obvious effects on the body weight of those mice were observed in each treatment group

Innovation Center of
Biotherapy, Chengdu, P. R.
China

⁹Department of Biology and
Biochemistry, Center for
Nuclear Receptors and Cell
Signaling, University of
Houston, Houston, U.S.A

¹⁰Department of Biosciences
and Nutrition at NOVUM,
Karolinska Institute, Solna,
Sweden

¹¹These authors contributed
equally

¹²Lead Contact

*Correspondence:
jgustafsson@uh.edu (J.-Å.G.),
taotaovip2005@163.com,
shengtaozhou@scu.edu.cn
(S.Z.)

<https://doi.org/10.1016/j.isci.2020.101458>

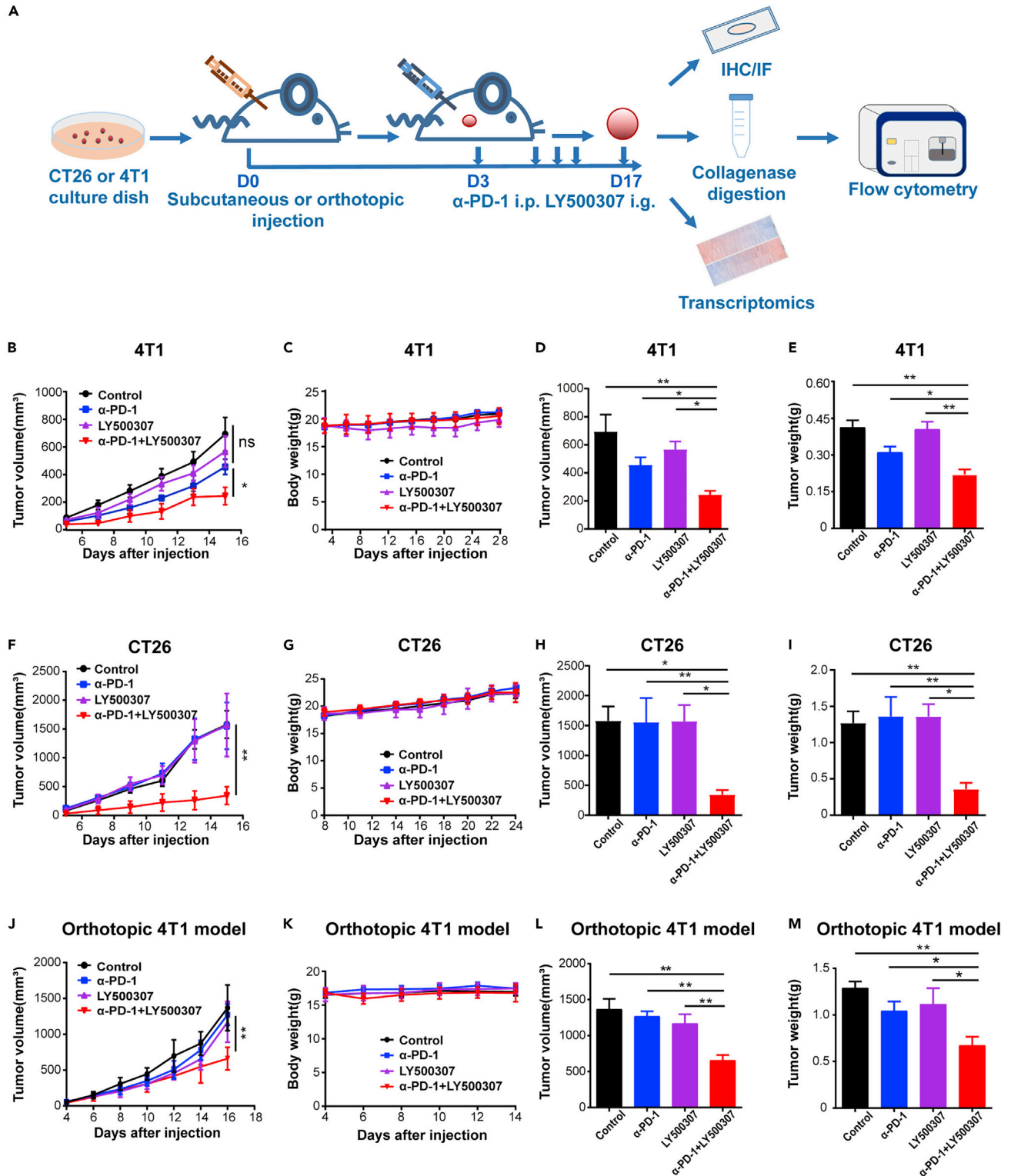


Figure 1. Selective ER β agonist LY500307 Overcomes ICB Therapy Resistance in Tumors

(A) Schematic model for the evaluation of ER β activation in ICB-resistant tumors and the integrative analytical strategy for underlying molecular mechanisms. (B) BALB/c mice were injected subcutaneously with 4T1 cells and each treatment was given at the indicated time. Growth kinetics was recorded at indicated time (n = 4–5 for each group).

Figure 1. Continued

- (C) The body weight of 4T1 murine model in each group at indicated time points (n = 5 for each group).
 - (D) The tumor volume of 4T1 murine model in each group at 15th day after tumor injection (n = 4–5 for each group).
 - (E) The tumor weight of 4T1 murine model in each group at 15th day after tumor injection (n = 5 for each group).
 - (F) BALB/c mice were injected subcutaneously with CT26 cells and each treatment was given at the indicated time. Growth kinetics was recorded at indicated time (n = 4 for each group).
 - (G) The body weight of CT26 murine model in each group at indicated time points (n = 5 for each group).
 - (H) The tumor volume of CT26 murine model in each group at 15th day after tumor injection (n = 4 for each group).
 - (I) The tumor weight of CT26 murine model in each group at 15th day after tumor injection (n = 4 for each group).
 - (J) BALB/c mice were orthotopically injected with 4T1 cells and each treatment was given at the indicated time. Growth kinetics was recorded at indicated time (n = 5 for each group).
 - (K) The body weight of orthotopic 4T1 murine model in each group at indicated time points (n = 5 for each group).
 - (L) The tumor volume of orthotopic 4T1 murine model in each group at 16th day after tumor injection (n = 5 for each group).
 - (M) The tumor weight of orthotopic 4T1 murine model in each group at 16th day after tumor injection (n = 5 for each group).
- Data are shown as mean ± SEM. One-way ANOVA, *, p < 0.05; **, p < 0.01.

(Figure S3J). Altogether, these data suggest that combination of ERβ activation and ICB therapy enhances therapeutic efficacy in TNBC and colorectal cancers.

Combined Therapy of ERβ Activation and ICB Therapy Reduces MDSC Infiltration and Increases Cytotoxic T Lymphocytes *In Vivo*

To investigate the underlying mechanisms for the enhanced therapeutic efficacy of combined therapy, we performed RNA sequencing (RNA-seq) analysis for the bulk tumors of the four groups of 4T1 mouse models. Similar transcriptional changes were observed within each replicate of the four models (Figure 2A). Unsupervised clustering by PCA analysis showed that each replicate consistently showed altered transcriptional profiles (Figure 2B). In addition, the statistically significantly altered genes between the combination treatment group with tumors treated with either drug as a monotherapy were also demonstrated (Figures S4A and S4B). Interestingly, gene ontology (GO) enrichment identified a list of pathways associated with immune alterations. Among those top enriched pathways, we found that a group of T cell-related pathways were up-regulated in the combined therapy group, including T cell proliferation, T cell receptor signaling pathway, interferon gamma response, and TNF-α signaling via NF-κB, whereas a group of enriched pathways involved in myeloid cell differentiation and activation were found to be dramatically down-regulated in the combined therapy group (Figure 2C). Therefore, we further investigated which subtype of myeloid cells in the tumor beds are significantly changed by combined treatment of ERβ activation and PD-1 antibody. After screening for a number of subtypes of myeloid cells (including neutrophils, macrophages, eosinophils, basophils, and MDSCs) using flow cytometry, we found that only the number of MDSCs (CD45⁺CD11b⁺Gr1⁺ cells) was dramatically reduced in the combined treatment group in three *in vivo* tumor models (Figures 2D–2F and S5A). Further flow cytometry analysis revealed that, in the combined treatment group, the number of CD8⁺ T cells was dramatically increased compared with monotherapy and control groups in three *in vivo* tumor models (Figures S5B and S6A–S6C). Thus, combined therapy with ERβ activation and PD-1 antibody suppresses MDSC infiltration and increases cytotoxic T lymphocytes in the tumor beds.

CSF1R⁺ MDSCs Infiltrate in Tumor Beds and MDSC Depletion Enhances ICB Therapy

We next explored the mechanisms for MDSC infiltration in these tumors. As previous reports demonstrated that the CSF1/CSF1R axis was crucial for the chemotaxis of MDSCs into the tumor microenvironment (Kumar et al., 2017; Neubert et al., 2018; Soncin et al., 2018; Xu et al., 2013; Zhu et al., 2014) and CSF1 signatures could be predictive in breast cancer (Beck et al., 2009; DeNardo et al., 2011), we further examined whether CSF1R⁺ MDSCs played a role in ERβ activation-mediated suppression of ICB therapy-resistant tumors. Immunofluorescent analysis revealed a number of CSF1R⁺Gr1⁺ cells in the control group of both 4T1 and CT26 subcutaneous tumor models (Figures 3A and 3B). Although no significant changes were observed in the PD-1 antibody monotherapy group (Figures 3A and 3B), the number of infiltrated CSF1R⁺Gr1⁺ cells in the combined anti-PD-1/LY500307 treatment group was significantly reduced in both models (Figures 3A and 3B). These findings further indicated that ERβ activation reduced CSF1R⁺ MDSCs in the ICB-resistant tumors to regain sensitivity to ICB therapy.

We next characterized the functional role of MDSCs in the development of resistance to ICB therapy. MDSC depletion using Gr1 antibody *in vivo* significantly decreased infiltration of MDSCs in PD-1

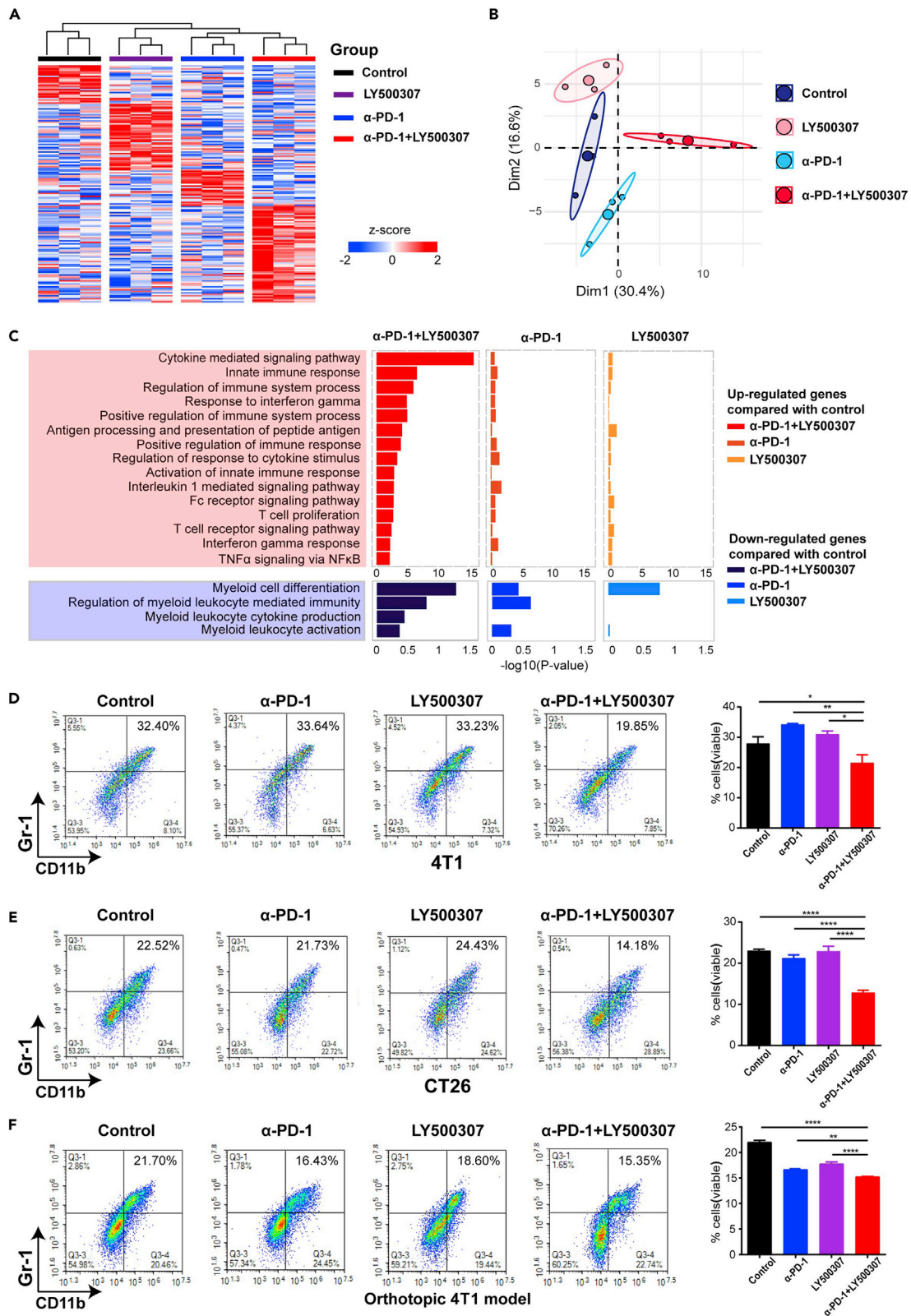


Figure 2. Integrative Analysis Identifies MDSCs as the Target Cell Types for ER β Activation in ICB-Resistant Tumors

- (A) Heatmap of the differentially expressed genes in each treatment group of 4T1 model.
 (B) Principal component analysis (PCA) of RNA-seq data from each treatment group of 4T1 model.
 (C) GO enrichment analysis comparing indicated treatment groups using the RNA-seq data.
 (D) Flow cytometry analysis of Gr1⁺CD11b⁺ cells in the subcutaneous tumors in each treatment group of 4T1 model (n = 3 for each group).
 (E) Flow cytometry analysis of Gr1⁺CD11b⁺ cells in the subcutaneous tumors in each treatment group of CT26 model (n = 3–5 for each group).
 (F) Flow cytometry analysis of Gr1⁺CD11b⁺ cells in the orthotopic tumors in each treatment group of 4T1 model (n = 3–4 for each group).
 Data are shown as mean \pm SEM; one-way ANOVA, *, p < 0.05; **, p < 0.01; ****, p < 0.0001.

antibody-treated 4T1 and CT26 subcutaneous tumor models, similar to that of the combined anti-PD-1/LY500307 treatment group (Figures 3A and 3B). Functionally, MDSC depletion enhanced the sensitivity of 4T1 cells to ICB therapy, as revealed in the growth curve in each treatment group (Figure 3C), tumor volume (Figure 3E), and tumor weight (Figure 3F), without affecting mouse weight *in vivo* (Figure 3D). This effect is comparable with combined treatment with LY500307 and ICB therapy but significantly better than any of the monotherapy regimens (Figure 3C). Similar results were also observed in the CT26 tumor model *in vivo* (Figures 3G–3J). These results demonstrated that CSF1R⁺ MDSCs infiltrate in tumor beds and MDSC depletion enhances ICB therapy.

Tumor Cells Secrete CSF1 to Attract CSF1R⁺ MDSC Infiltration

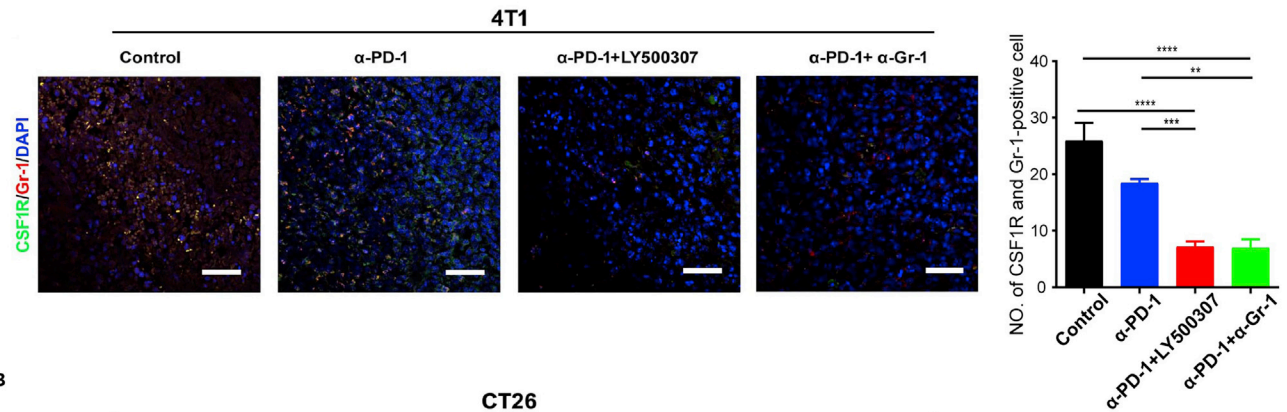
We assessed how CSF1R⁺ MDSCs infiltrated into tumor beds. We performed a Raybio cytokine array analysis to characterize the alteration of cytokines and chemokines in 4T1 cells treated with LY500307 (Figure S7A). It was demonstrated that, among all the down-regulated chemokines and cytokines, the expressions of M-CSF (CSF-1), CXCL9, CCL19, CXCL4, CCL1, TNF α , and VEGFA were reduced for over 30% percent (Figure S7B). By contrast, the expressions of TNFSF8, IL5, CXCL1, LIX, and CD62L were up-regulated after treatment with LY500307 in 4T1 cells (Figure S7C). This result led us to further characterize the functional role of tumor-derived CSF1 as a chemoattractant for CSF1R⁺ in tumor beds (Figure 4A). Tumors derived from both 4T1 and CT26 cells overexpress CSF1 compared with normal mouse breast and colorectal tissues, respectively (Figures 4B and 4C). We next examined whether ER β activation could have any effects on the expression levels of CSF1 in the two cell lines. Treatment with LY500307 caused remarkable reduction of CSF1 in both models, as measured by qPCR (Figures 4D and 4E) and ELISA analysis (Figures 4F and 4G). These observations indicate that ER β activation could lead to decreased release of CSF1 in tumor cells.

Subsequently, we explored whether the supernatants from 4T1 cells and CT26 cells could exert chemotactic effects for CSF1R⁺ MDSCs and whether blockade of CSF1/CSF1R axis could abolish these chemotactic effects *in vitro* (Figure 4H). The supernatant from control 4T1 cells and CT26 cells could attract CSF1R⁺ MDSCs to migrate to the lower layer of the Transwell chamber (Figures 4I and 4J). The number of CSF1R⁺ MDSCs attracted by the supernatants added with LY500307 was comparable with those in the control group in both models. However, the number of CSF1R⁺ MDSCs attracted by the supernatants from either LY500307-treated 4T1 or CT26 cells was significantly decreased, mimicked by the blockade of CSF1/CSF1R axis using CSF1R neutralization antibody *ex vivo* (Figures 4I and 4J). We further characterized the functional phenotype of MDSCs isolated from murine tumor tissues in each treatment group. It was revealed that the expression of genes encoding for TLR4, CD80, and CD86 molecules related to a pro-inflammatory phenotype was significantly increased in MDSCs of the combined treatment group with PD-1 antibody and LY500307, whereas IDO and NOS gene expressions, which are known to inhibit anti-tumor T cell responses, were reduced in MDSCs of the combined treatment group (Figures 4K–4M). Therefore, we concluded that LY500307 treatment could block the CSF1/CSF1R axis that mediated CSF1R⁺ MDSC infiltration in the ICB therapy-resistant tumors.

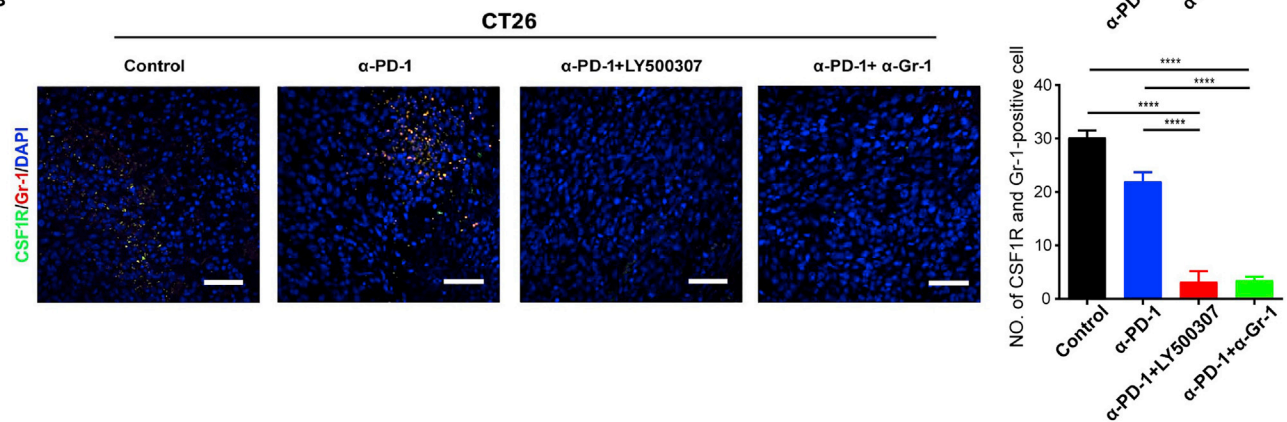
Blockade of CSF1R Mimics the Therapeutic Effects of ER β Activation for PD-1-Resistant Tumors

We explored whether ER β activation in ICB-resistant tumors could be mimicked by CSF1R blockade *in vivo*. We found that combined therapy of PD-1 antibody and CSF1R antibody *in vivo* remarkably attenuated the growth of 4T1 cells, with similar efficacy as combined therapy of PD-1 antibody and LY500307 (Figure 5A), without affecting mouse body weight (Figure 5B). These therapeutic effects were also revealed in the tumor volume (Figure 5C) and tumor weight at indicated time point (Figure 5D). Likewise, combined therapy of PD-1 antibody and CSF1R antibody also potentially impaired CT26 tumor growth *in vivo*, comparable with

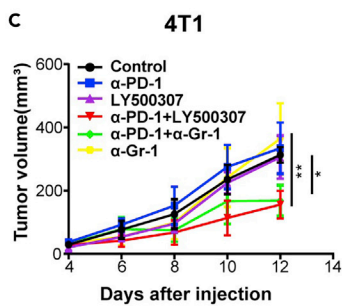
A



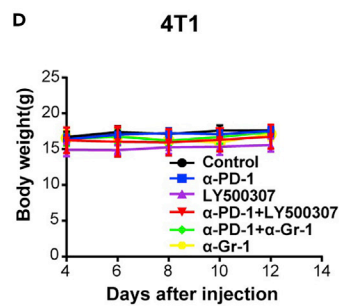
B



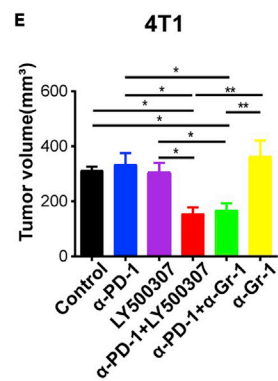
C



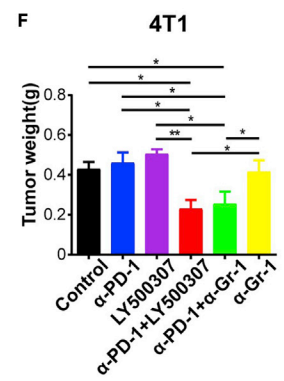
D



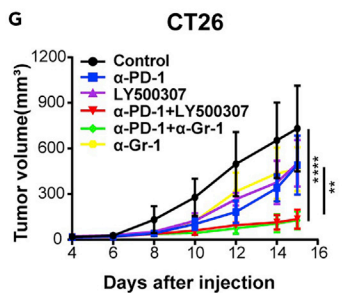
E



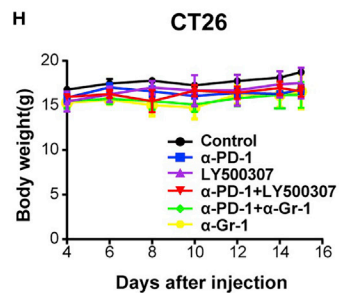
F



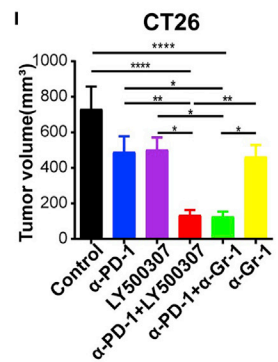
G



H



I



J

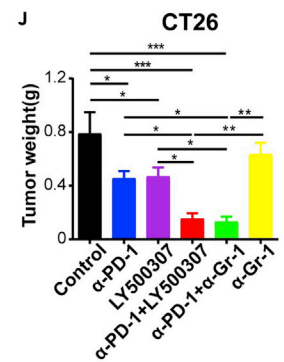


Figure 3. ERβ Activation Mimics Depletion of MDSCs in ICB-Resistant Tumors

- (A) Immunofluorescent analysis of abundance of CSF1R⁺Gr1⁺ in different treatment groups in 4T1 mouse model (n = 4 for each group).
 - (B) Immunofluorescent analysis of abundance of CSF1R⁺Gr1⁺ in different treatment groups in CT26 mouse model (n = 4 for each group).
 - (C) BALB/c mice were injected subcutaneously with 4T1 cells and each treatment was given at the indicated time. Growth kinetics was recorded at indicated time (n = 4 for each group).
 - (D) The body weight of 4T1 murine model in each group at indicated time points (n = 5 for each group).
 - (E) The tumor volume of 4T1 murine model in each group at 12th day after tumor injection (n = 4 for each group).
 - (F) The tumor weight of 4T1 murine model in each group at 12th day after tumor injection (n = 4 for each group).
 - (G) BALB/c mice were injected subcutaneously with CT26 cells and each treatment was given at the indicated time. Growth kinetics was recorded at indicated time (n = 5 for each group).
 - (H) The body weight of CT26 murine model in each group at indicated time points (n = 4 for each group).
 - (I) The tumor volume of CT26 murine model in each group at 15th day after tumor injection (n = 5 for each group).
 - (J) The tumor weight of CT26 murine model in each group at 15th day after tumor injection (n = 5 for each group).
- Data are shown as mean ± SEM; one-way ANOVA, *, p < 0.05; **, p < 0.01; ***, p < 0.001; ****, p < 0.0001.

that of combined therapy group of PD-1 antibody and LY500307, as shown by growth curve (Figure 5E), tumor volume (Figure 5G), and tumor weight at indicated time (Figure 5H). No impact of these treatments on mouse body weight was observed in CT26 models as well (Figure 5F). These data suggested that CSF1R blockade combined with PD-1 antibody therapy showed similar therapeutic effects with the combined therapy of ERβ activation and PD-1 antibody.

CSF1/CSF1R Axis Is Activated in Patients with TNBC and Colorectal Cancer and Informs Clinical Prognosis

Clinically, we examined the expression patterns of CSF1 and CSF1R in TNBC and colorectal cancer patient samples. We found that in TNBC clinical samples, the expression of CSF1 was primarily located in the epithelial cytoplasm (Figure 6A) and was up-regulated compared with normal breast tissue (Figures 6C and 6E). The expression of CSF1R, however, was primarily restricted to the stromal compartment (Figure 6A) and was overexpressed in TNBC clinical samples compared with normal breast tissue as well (Figures 6D and 6F). Similarly, in colorectal cancer clinical samples, CSF1 expression was also restricted to the epithelial cytoplasm (Figure 6B) and overexpressed compared with normal colorectal tissue (Figures 6G and 6I). CSF1R expression was located to the stromal cells (Figure 6B) and was overexpressed in patients with colorectal cancer compared with normal colorectal tissue (Figures 6H and 6J).

We further investigated whether CSF1/CSF1R axis has any impact on patient prognosis. Colorectal cancer was used as an example to examine the correlation of expression of CSF1 and CSF1R with prognosis in public datasets. We found that, in GSE39582 dataset, both CSF1 (hazard ratio [HR] = 1.83(1.08–3.11), p = 2.21 × 10⁻²) and CSF1R (HR = 2.55(1.47–4.4), p = 4.99 × 10⁻⁴) overexpression was correlated with poorer relapse-free survival (RFS) in stage II colorectal patients (Figures S8A and S8B). This indicated that CSF1/CSF1R axis informs clinical prognosis in patients with cancer. Altogether, these data give support to our finding that combined therapy of ERβ activation and ICB could possibly suppress CSF1/CSF1R axis to impair MDSC infiltration and increase CD8⁺ T cells recruitment to tumor beds, which overcame the resistance to ICB therapy in tumors.

DISCUSSION

Traditional cancer therapies include surgery, chemotherapy, radiotherapy, and molecularly targeted regimens. Recently, the discovery of immune checkpoint molecules has not only led to paradigm shift of our understanding of immune system but also offered a novel therapeutic option for patients with cancer: ICB therapy (Kalbasi and Ribas, 2019). The therapeutic antibody ipilimumab, targeting CTLA-4 as the first checkpoint inhibitor to be approved for patients with cancer in the clinical setting (Lo and Abdel-Motal, 2017; Rowshanravan et al., 2018), whereas the second immune checkpoint receptor, PD-1, which is expressed by activated T cells, is also considered important for driving T cells into an “exhausted” state (Blank et al., 2019; Wherry and Kurachi, 2015). Blocking either CTLA-4 or PD-1 has led to unprecedented durable responses with a generally favorable toxicity profile (Spallarossa et al., 2018). However, it is reported in large clinical trials that only a fraction of patients respond and many will relapse (Nishino et al., 2017). This has led to continuous investigation of mechanisms that lead to ICB therapy resistance and strategies to overcome the resistance (Minn and Wherry, 2016; Patel and Minn, 2018). For instance, Ishizuka et al. (2019) recently found that loss of function of the RNA-editing enzyme ADAR1 in tumor cells remarkably sensitizes tumors to immunotherapy and overcomes resistance to ICB. Mechanistically, in the absence of

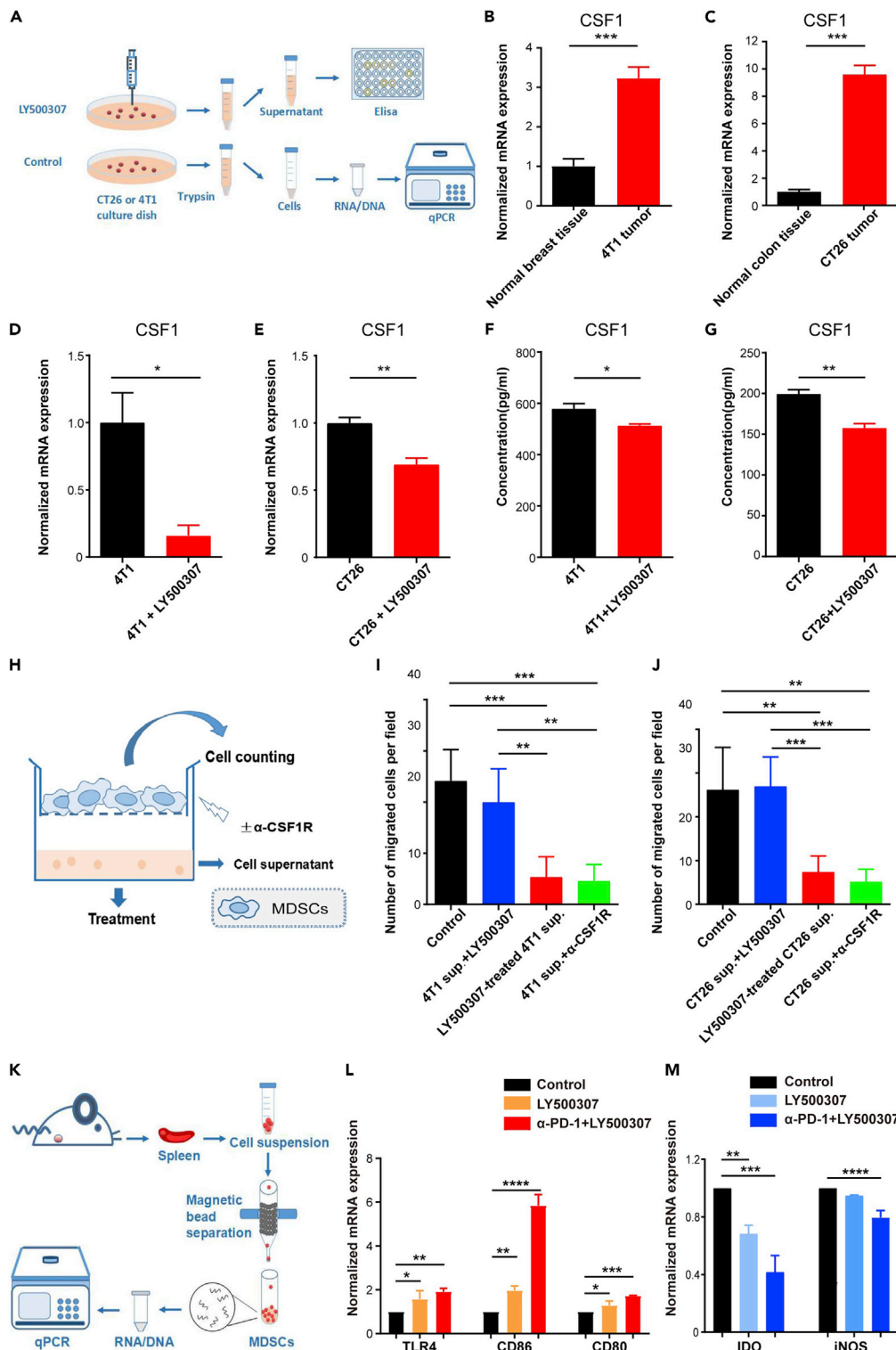


Figure 4. ER β Activation Reduces Tumor Cell-Derived CSF1 and Blocks MDSC Chemotaxis via CSF1/CSF1R Axis

(A) Schematic model describing the procedure to analyze the mRNA levels or supernatant protein concentration of CSF1 in indicated samples.

(B) The CSF1 mRNA levels between normal mouse breast tissues and 4T1 tumor tissues.

(C) The CSF1 mRNA levels between normal colon tissues and CT26 tumor tissues.

Figure 4. Continued

- (D) The CSF1 mRNA levels between control 4T1 cells and LY500307-treated 4T1 cells.
 - (E) The CSF1 mRNA levels between control CT26 cells and LY500307-treated CT26 cells.
 - (F) The CSF1 concentration in the supernatant of 4T1 cells and LY500307-treated 4T1 cells.
 - (G) The CSF1 concentration in the supernatant of CT26 cells and LY500307-treated CT26 cells.
 - (H) Schematic model illustrating the MDSC chemotaxis assay.
 - (I) The number of migrated MDSCs in each treatment group of 4T1 *ex vivo* model using Transwell chamber assay.
 - (J) The number of migrated MDSCs in each treatment group of CT26 *ex vivo* model using Transwell chamber assay.
 - (K) Schematic model illustrating how we examined the expression of functional molecules in MDSCs.
 - (L) The expression of up-regulated genes of MDSCs in combined treatment group (n = 3 for each group).
 - (M) The expression of down-regulated genes of MDSCs in combined treatment group (n = 3 for each group).
- Data are shown as mean \pm SEM; one-way ANOVA, *, p < 0.05; **, p < 0.01; ***, p < 0.001, ****, p < 0.0001.

ADAR1, A-to-I editing of interferon-inducible RNA species is reduced, resulting in double-stranded RNA ligand sensing by PKR and MDA5, resulting in growth inhibition and tumor inflammation, respectively. Loss of ADAR1 overcomes resistance to PD-1 checkpoint blockade caused by inactivation of antigen presentation by tumor cells. More efforts are ongoing to find novel ways to battle against ICB resistance in patients with cancer. Our study demonstrated that combined therapy with an ER β agonist and PD-1 antibody showed synergistic effects for tumor treatment compared with monotherapies.

MDSCs represent a heterogeneous subset of myeloid cells with major regulatory functions, which play important roles in diseases, including cancer, autoimmune disease, cardiovascular diseases, and metabolic disorders (Gabrilovich, 2017; Kumar et al., 2016; Pawelec et al., 2019). Specifically, the immuno-regulatory functions of MDSCs are critical for hallmarks of cancer (Kumar et al., 2016). For instance, Calcinotto et al. (2018) reported that MDSCs could secrete IL-23 to drive castration-resistant prostate cancer (CRPC) progression in mice and patients with CRPC. IL-23 secreted by MDSCs can activate the androgen receptor pathway in prostate tumor cells, promoting cell survival and proliferation in androgen-deprived conditions. MDSCs also impact on the therapeutic efficacy of ICB therapy. Sun et al. (2019) demonstrated that tumor-infiltrating CXCR2⁺ neutrophilic MDSCs (PMN-MDSCs) may prevent optimal responses following both PD-axis ICB and adoptive T cell transfer therapy. Abolishment of PMN-MDSC trafficking with SX-682 enhances T cell-based immunotherapeutic efficacy and may be of benefit to patients with MDSC-infiltrated cancers. Moreover, Zhu et al. demonstrated that CSF1R can functionally reprogram myeloid responses that enhance antigen presentation and productive antitumor T cell responses and synergize with ICB treatment to elicit tumor regressions in pancreatic ductal adenocarcinoma (Zhu et al., 2014). These are consistent with our results that inhibition of MDSC infiltration by selective ER β agonist, possibly through suppression of CSF1/CSF1R axis, in the tumor microenvironment could potentially overcome ICB therapy resistance.

ER β , which is different from ER α , is primarily involved in the control of epithelial proliferation, neurodegeneration, and immune functions. Its tumor-suppressive functions have made ER β agonists potential therapeutic options for patients with cancer (Nikolos et al., 2018; Zhao et al., 2019). Our group recently demonstrated that selective ER β agonist LY500307 could suppress lung metastasis of TNBC and melanoma (Zhao et al., 2018). Mechanistically, although we observed that LY500307 potentially induced cell death of cancer cells metastasized to lung *in vivo*, it does not mediate apoptosis of cancer cells *in vitro*, indicating that the cell death-inducing effects of LY500307 might be mediated by the tumor microenvironment. Further functional analysis indicated that LY500307 treatment induced significant infiltration of neutrophils in the metastatic niche. LY500307-treated cancer cells increased neutrophil chemotaxis and *in vivo* neutrophil depletion by administration of anti-Ly6G antibody could reverse the effects of LY500307-mediated metastasis suppression. LY500307 could induce up-regulation of IL-1 β in TNBC and melanoma cells, which further triggered antitumor neutrophil chemotaxis. LY500307-mediated suppression of lung metastasis was attenuated in *Il1b*^{-/-} murine models. The present study has provided another example of immune-modulatory function of ER β activation in the treatment of cancer. Another interesting finding by the present study is that, from the RNA sequencing studies, a cluster of genes were uniquely up-regulated in tumors treated with combination therapy compared with each drug individually as a monotherapy. This set of genes might account for improved therapeutic effects for tumors compared with other monotherapy regimens.

Collectively, our study has identified a CSF1/CSF1R axis between cancer cells and MDSCs in the tumor microenvironment that ER β activation could potentially target for the treatment of ICB-resistant tumors. This provides the rationale for the combined use of selective ER β agonists and immune checkpoint inhibitors in patients with cancer.

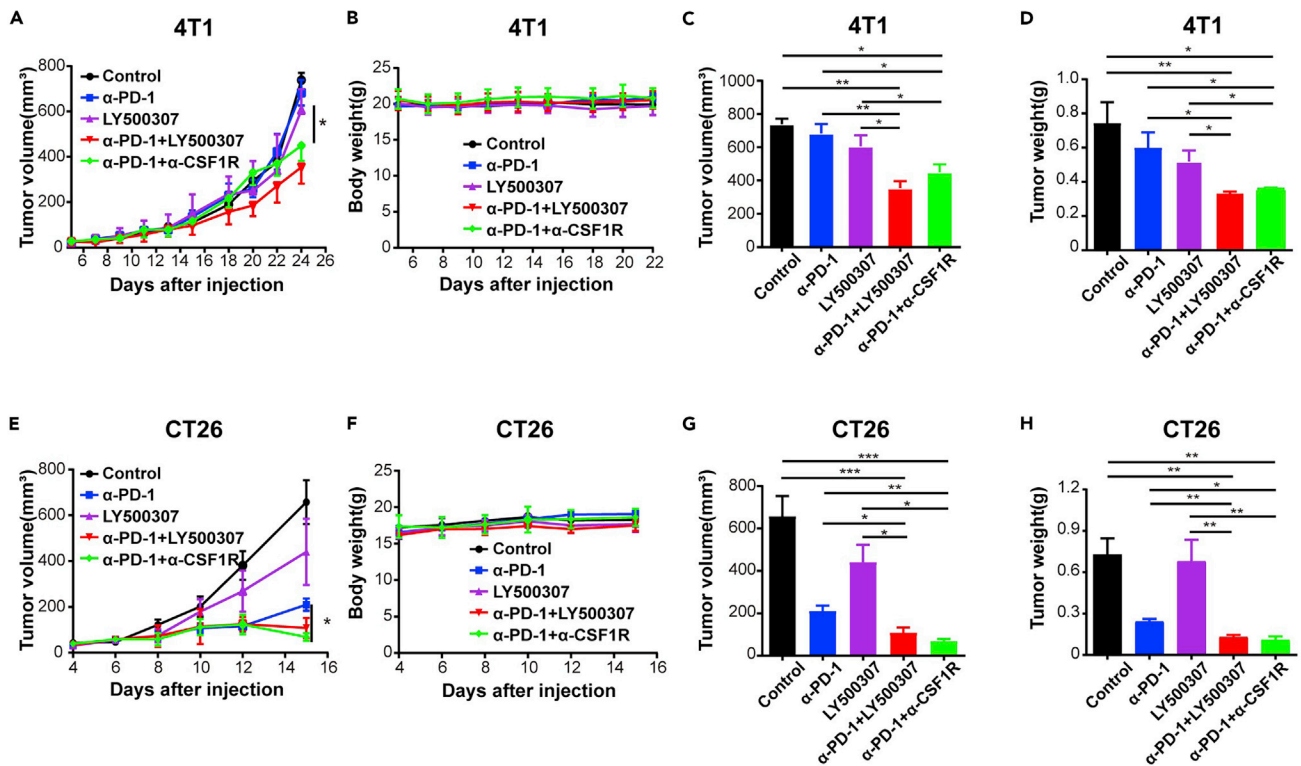


Figure 5. ER β Activation Overcomes ICB Resistance via CSF1/CSF1R Axis In Vivo

(A) BALB/c mice were injected subcutaneously with 4T1 cells and each treatment was given at the indicated time. Growth kinetics was recorded at indicated time (n = 5 for each group).

(B) The body weight of 4T1 murine model in each group at indicated time points (n = 5 for each group).

(C) The tumor volume of 4T1 murine model in each group at 24th day after tumor injection (n = 3 for each group).

(D) The tumor weight of 4T1 murine model in each group at 24th day after tumor injection (n = 4 for each group).

(E) BALB/c mice were injected subcutaneously with CT26 cells and each treatment was given at the indicated time. Growth kinetics was recorded at indicated time (n = 5 for each group).

(F) The body weight of CT26 murine model in each group at indicated time points (n = 5 for each group).

(G) The tumor volume of CT26 murine model in each group at 15th day after tumor injection (n = 3–5 for each group).

(H) The tumor weight of CT26 murine model in each group at 15th day after tumor injection (n = 3–4 for each group).

Data are shown as mean \pm SEM; one-way ANOVA, *, p < 0.05; **, p < 0.01; ***, p < 0.001;.

Limitations of the Study

The limitations of the study include that the number of clinical samples included in this study is relatively small, which we might enlarge in the future investigations. Another drawback is that two cancer mouse models that are resistant to ICB therapy are used in this study.

Resource Availability

Lead Contact

Further information could be obtained by contacting the Lead Contact, Shengtao Zhou (shengtaozhou@scu.edu.cn).

Materials Availability

Materials are available upon request from Dr. Shengtao Zhou.

Data and Code Availability

RNA sequencing data have been deposited in the Gene Expression Omnibus (GEO) database under accession number GSE132529.

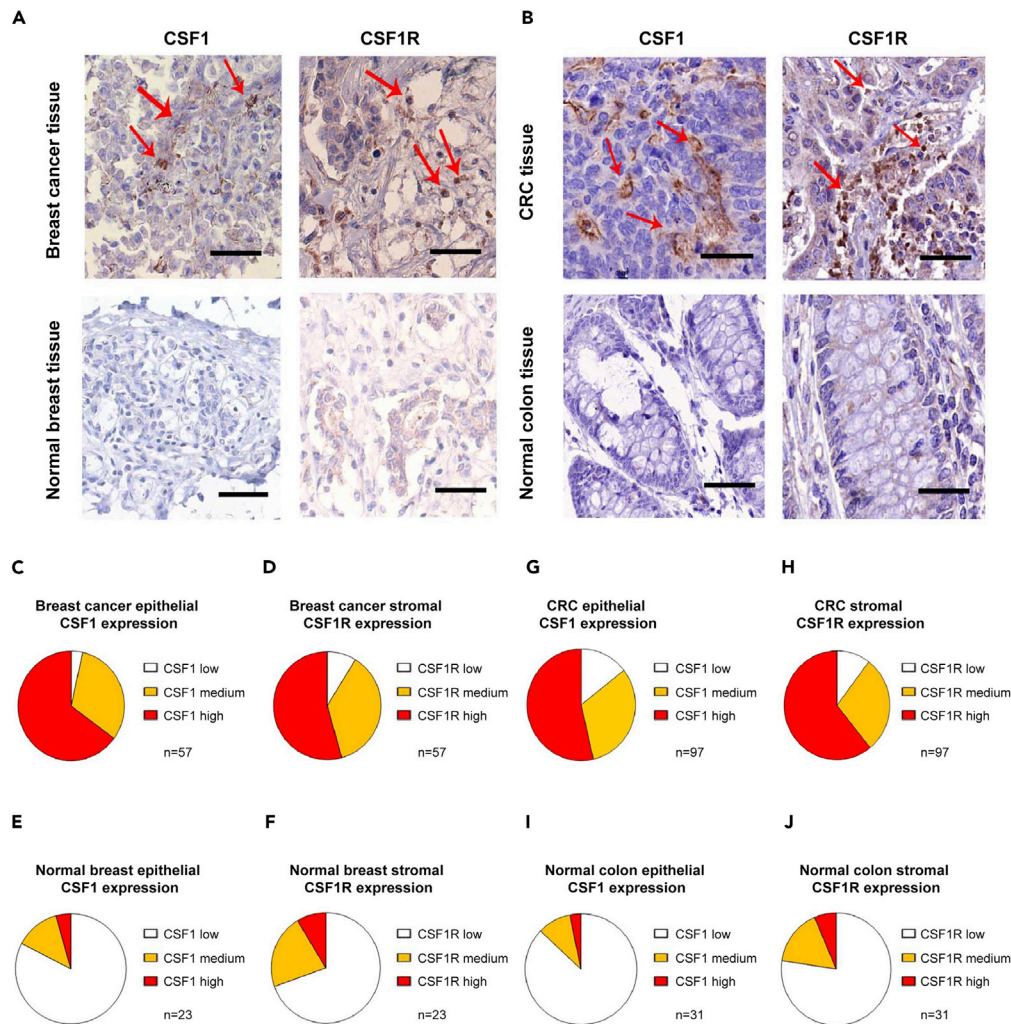


Figure 6. The Expression of CSF1/CSF1R in Human TNBC and CRC Samples

(A) Immunohistochemistry analysis of CSF1 and CSF1R in human TNBC and normal breast tissue samples.
 (B) Immunohistochemistry analysis of CSF1 and CSF1R in human colorectal cancer and normal colon tissue samples.
 (C) The distribution of CSF1 expression in breast cancer epithelial cells.
 (D) The distribution of CSF1R expression in breast cancer stromal cells.
 (E) The distribution of CSF1 expression in normal breast epithelial cells.
 (F) The distribution of CSF1R expression in normal breast stromal cells.
 (G) The distribution of CSF1 expression in CRC epithelial cells.
 (H) The distribution of CSF1R expression in CRC stromal cells.
 (I) The distribution of CSF1 expression in normal colon epithelial cells.
 (J) The distribution of CSF1R expression in normal colon stromal cells.
 The red arrows point to the immunopositive cells.

METHODS

All methods can be found in the accompanying [Transparent Methods supplemental file](#).

SUPPLEMENTAL INFORMATION

Supplemental Information can be found online at <https://doi.org/10.1016/j.isci.2020.101458>.

ACKNOWLEDGMENTS

This work was supported by grants from National Natural Science Foundation of China (grant #81822034, grant # 81821002, and grant #81773119), National Key Research and Development Program of China (grant

#2018YFA0109200 and grant #2017YFA0106800), Sichuan Science-Technology International Cooperation Project (grant #2019YFH0144), Direct Scientific Research Grants from West China Second Hospital, Sichuan University (grant #KS021, grant #K1907, and grant KX247), the Robert A Welch Foundation for a grant (grant #E-0004), the Swedish Cancer Foundation, the Center for Innovative Medicine and the Novo Nordisk Fund.

AUTHOR CONTRIBUTIONS

Conceptualization, H.H., J.-A.G. and S.Z.; Methodology, S.H., N.Z., J.-A.G. and S.Z.; Investigation, S.H., N.Z., B.S., J.Y., Q.Z., S.Z., X.J., Z.C., P.Z., and Y.Z.; Formal analysis, W.W., L.Z., R.C.G., J.-A.G. and S.Z.; Writing – Original Draft, S.H., N.Z., J.-A.G. and S.Z.; Writing – Review and Editing, L.Z., R.C.G., Y.H.A., H.H., J.-A.G. and S.Z.; Supervision, H.H., J.-A.G. and S.Z.; Funding Acquisition, H.H., J.-A.G. and S.Z.

DECLARATION OF INTERESTS

No competing interests were declared.

Received: January 29, 2020

Revised: July 8, 2020

Accepted: August 10, 2020

Published: September 25, 2020

REFERENCES

- Beck, A.H., Espinosa, I., Edris, B., Li, R., Montgomery, K., Zhu, S., Varma, S., Marinelli, R.J., van de Rijn, M., and West, R.B. (2009). The macrophage colony-stimulating factor 1 response signature in breast carcinoma. *Clin. Cancer Res.* 15, 778–787.
- Blank, C.U., Haining, W.N., Held, W., Hogan, P.G., Kallies, A., Lugli, E., Lynn, R.C., Philip, M., Rao, A., Restifo, N.P., et al. (2019). Defining ‘T cell exhaustion’. *Nat. Rev. Immunol.* 19, 665–674.
- Calcinotto, A., Spataro, C., Zagato, E., Di Mitri, D., Gil, V., Crespo, M., De Bernardis, G., Losa, M., Mirenda, M., Pasquini, E., et al. (2018). IL-23 secreted by myeloid cells drives castration-resistant prostate cancer. *Nature* 559, 363–369.
- Conway, J.R., Kofman, E., Mo, S.S., Elmarakeby, H., and Van Allen, E. (2018). Genomics of response to immune checkpoint therapies for cancer: implications for precision medicine. *Genome Med.* 10, 93.
- DeNardo, D.G., Brennan, D.J., Rexhepaj, E., Ruffell, B., Shiao, S.L., Madden, S.F., Gallagher, W.M., Wadhvani, N., Keil, S.D., Junaid, S.A., et al. (2011). Leukocyte complexity predicts breast cancer survival and functionally regulates response to chemotherapy. *Cancer Discov.* 1, 54–67.
- Fritz, J.M., and Lenardo, M.J. (2019). Development of immune checkpoint therapy for cancer. *J. Exp. Med.* 216, 1244–1254.
- Gabrilovich, D.I. (2017). Myeloid-derived suppressor cells. *Cancer Immunol. Res.* 5, 3–8.
- Gopalakrishnan, V., Spencer, C.N., Nezi, L., Reuben, A., Andrews, M.C., Karpinet, T.V., Prieto, P.A., Vicente, D., Hoffman, K., Wei, S.C., et al. (2018). Gut microbiome modulates response to anti-PD-1 immunotherapy in melanoma patients. *Science* 359, 97–103.
- Gordon, S.R., Maute, R.L., Dulken, B.W., Hutter, G., George, B.M., McCracken, M.N., Gupta, R., Tsai, J.M., Sinha, R., Corey, D., et al. (2017). PD-1 expression by tumour-associated macrophages inhibits phagocytosis and tumour immunity. *Nature* 545, 495–499.
- Ibrahim, A., Hugerth, L.W., Hases, L., Saxena, A., Seifert, M., Thomas, Q., Gustafsson, J.A., Engstrand, L., and Williams, C. (2019). Colitis-induced colorectal cancer and intestinal epithelial estrogen receptor beta impact gut microbiota diversity. *Int. J. Cancer* 144, 3086–3098.
- Ishizuka, J.J., Manguso, R.T., Cheruiyot, C.K., Bi, K., Panda, A., Iracheta-Velvet, A., Miller, B.C., Du, P.P., Yates, K.B., Dubrot, J., et al. (2019). Loss of ADAR1 in tumours overcomes resistance to immune checkpoint blockade. *Nature* 565, 43–48.
- Kalbasi, A., and Ribas, A. (2019). Tumour-intrinsic resistance to immune checkpoint blockade. *Nat. Rev. Immunol.* 20, 25–39.
- Keenan, T.E., Burke, K.P., and Van Allen, E.M. (2019). Genomic correlates of response to immune checkpoint blockade. *Nat. Med.* 25, 389–402.
- Kim, K., Skora, A.D., Li, Z., Liu, Q., Tam, A.J., Blosser, R.L., Diaz, L.A., Jr., Papadopoulos, N., Kinzler, K.W., Vogelstein, B., et al. (2014). Eradication of metastatic mouse cancers resistant to immune checkpoint blockade by suppression of myeloid-derived cells. *Proc. Natl. Acad. Sci. U S A* 111, 11774–11779.
- Kumar, V., Donthireddy, L., Marvel, D., Condamine, T., Wang, F., Lavilla-Alonso, S., Hashimoto, A., Vonteddu, P., Behera, R., Goins, M.A., et al. (2017). Cancer-associated fibroblasts neutralize the anti-tumor effect of csf1 receptor blockade by inducing PMN-MDSC infiltration of tumors. *Cancer Cell* 32, 654–668.e5.
- Kumar, V., Patel, S., Tcyganov, E., and Gabrielovich, D.I. (2016). The nature of myeloid-derived suppressor cells in the tumor microenvironment. *Trends Immunol.* 37, 208–220.
- Lo, B., and Abdel-Motal, U.M. (2017). Lessons from CTLA-4 deficiency and checkpoint inhibition. *Curr. Opin. Immunol.* 49, 14–19.
- Minn, A.J., and Wherry, E.J. (2016). Combination cancer therapies with immune checkpoint blockade: convergence on interferon signaling. *Cell* 165, 272–275.
- Neubert, N.J., Schmittnaegel, M., Bordry, N., Nassiri, S., Wald, N., Martignier, C., Tille, L., Homicsko, K., Damsky, W., Maby-El Hajjami, H., et al. (2018). T cell-induced CSF1 promotes melanoma resistance to PD1 blockade. *Sci. Transl. Med.* 10, eaan3311.
- Nikolos, F., Thomas, C., Bado, I., and Gustafsson, J.A. (2018). ERbeta sensitizes NSCLC to chemotherapy by regulating DNA damage response. *Mol. Cancer Res.* 16, 233–242.
- Nishino, M., Ramaiya, N.H., Hatabu, H., and Hodi, F.S. (2017). Monitoring immune-checkpoint blockade: response evaluation and biomarker development. *Nat. Rev. Clin. Oncol.* 14, 655–668.
- Patel, S.A., and Minn, A.J. (2018). Combination cancer therapy with immune checkpoint blockade: mechanisms and strategies. *Immunity* 48, 417–433.
- Pauken, K.E., Dougan, M., Rose, N.R., Lichtman, A.H., and Sharpe, A.H. (2019). Adverse events following cancer immunotherapy: obstacles and opportunities. *Trends Immunol.* 40, 511–523.
- Pawelec, G., Verschoor, C.P., and Ostrand-Rosenberg, S. (2019). Myeloid-derived suppressor cells: not only in tumor immunity. *Front. Immunol.* 10, 1099.
- Pitt, J.M., Vetzizou, M., Daillere, R., Roberti, M.P., Yamazaki, T., Routy, B., Lepage, P., Boneca, I.G., Chamillard, M., Kroemer, G., et al. (2016). Resistance mechanisms to immune-checkpoint blockade in cancer: tumor-intrinsic and -extrinsic factors. *Immunity* 44, 1255–1269.

Reese, J.M., Bruinsma, E.S., Nelson, A.W., Chernukhin, I., Carroll, J.S., Li, Y., Subramaniam, M., Suman, V.J., Negron, V., Monroe, D.G., et al. (2018). ERbeta-mediated induction of cystatins results in suppression of TGFbeta signaling and inhibition of triple-negative breast cancer metastasis. *Proc. Natl. Acad. Sci. U S A* **115**, E9580–E9589.

Routy, B., Le Chatelier, E., Derosa, L., Duong, C.P.M., Alou, M.T., Daillere, R., Fluckiger, A., Messaoudene, M., Rauber, C., Roberti, M.P., et al. (2018). Gut microbiome influences efficacy of PD-1-based immunotherapy against epithelial tumors. *Science* **359**, 91–97.

Rowshanravan, B., Halliday, N., and Sansom, D.M. (2018). CTLA-4: a moving target in immunotherapy. *Blood* **131**, 58–67.

Sanmamed, M.F., and Chen, L. (2018). A paradigm shift in cancer immunotherapy: from enhancement to normalization. *Cell* **175**, 313–326.

Soncin, I., Sheng, J., Chen, Q., Foo, S., Duan, K., Lum, J., Poidinger, M., Zolezzi, F., Karjalainen, K., and Ruedl, C. (2018). The tumour microenvironment creates a niche for

the self-renewal of tumour-promoting macrophages in colon adenoma. *Nat. Commun.* **9**, 582.

Spallarossa, P., Meliota, G., Brunelli, C., Arboscello, E., Ameri, P., Dessalvi, C.C., Grossi, F., Deidda, M., Mele, D., Sarocchi, M., et al. (2018). Potential cardiac risk of immune-checkpoint blockade as anticancer treatment: what we know, what we do not know, and what we can do to prevent adverse effects. *Med. Res. Rev.* **38**, 1447–1468.

Sun, L., Clavijo, P.E., Robbins, Y., Patel, P., Friedman, J., Greene, S., Das, R., Silvin, C., Van Waes, C., Horn, L.A., et al. (2019). Inhibiting myeloid-derived suppressor cell trafficking enhances T cell immunotherapy. *JCI Insight* **4**, 126853.

Wherry, E.J., and Kurachi, M. (2015). Molecular and cellular insights into T cell exhaustion. *Nat. Rev. Immunol.* **15**, 486–499.

Williams, C., DiLeo, A., Niv, Y., and Gustafsson, J.A. (2016). Estrogen receptor beta as target for colorectal cancer prevention. *Cancer Lett.* **372**, 48–56.

Wykes, M.N., and Lewin, S.R. (2018). Immune checkpoint blockade in infectious diseases. *Nat. Rev. Immunol.* **18**, 91–104.

Xu, J., Escamilla, J., Mok, S., David, J., Priceman, S., West, B., Bollag, G., McBride, W., and Wu, L. (2013). CSF1R signaling blockade stanches tumor-infiltrating myeloid cells and improves the efficacy of radiotherapy in prostate cancer. *Cancer Res.* **73**, 2782–2794.

Zhao, L., Huang, S., Mei, S., Yang, Z., Xu, L., Zhou, N., Yang, Q., Shen, Q., Wang, W., Le, X., et al. (2018). Pharmacological activation of estrogen receptor beta augments innate immunity to suppress cancer metastasis. *Proc. Natl. Acad. Sci. U S A* **115**, E3673–E3681.

Zhao, L., Zhou, S., and Gustafsson, J.A. (2019). Nuclear receptors: recent drug discovery for cancer therapies. *Endocr. Rev.* **40**, 1207–1249.

Zhu, Y., Knolhoff, B.L., Meyer, M.A., Nywening, T.M., West, B.L., Luo, J., Wang-Gillam, A., Goedegebuure, S.P., Linehan, D.C., and DeNardo, D.G. (2014). CSF1/CSF1R blockade reprograms tumor-infiltrating macrophages and improves response to T-cell checkpoint immunotherapy in pancreatic cancer models. *Cancer Res.* **74**, 5057–5069.

Supplemental Information

Pharmacological Activation of Estrogen Receptor

Beta Overcomes Tumor Resistance to Immune

Checkpoint Blockade Therapy

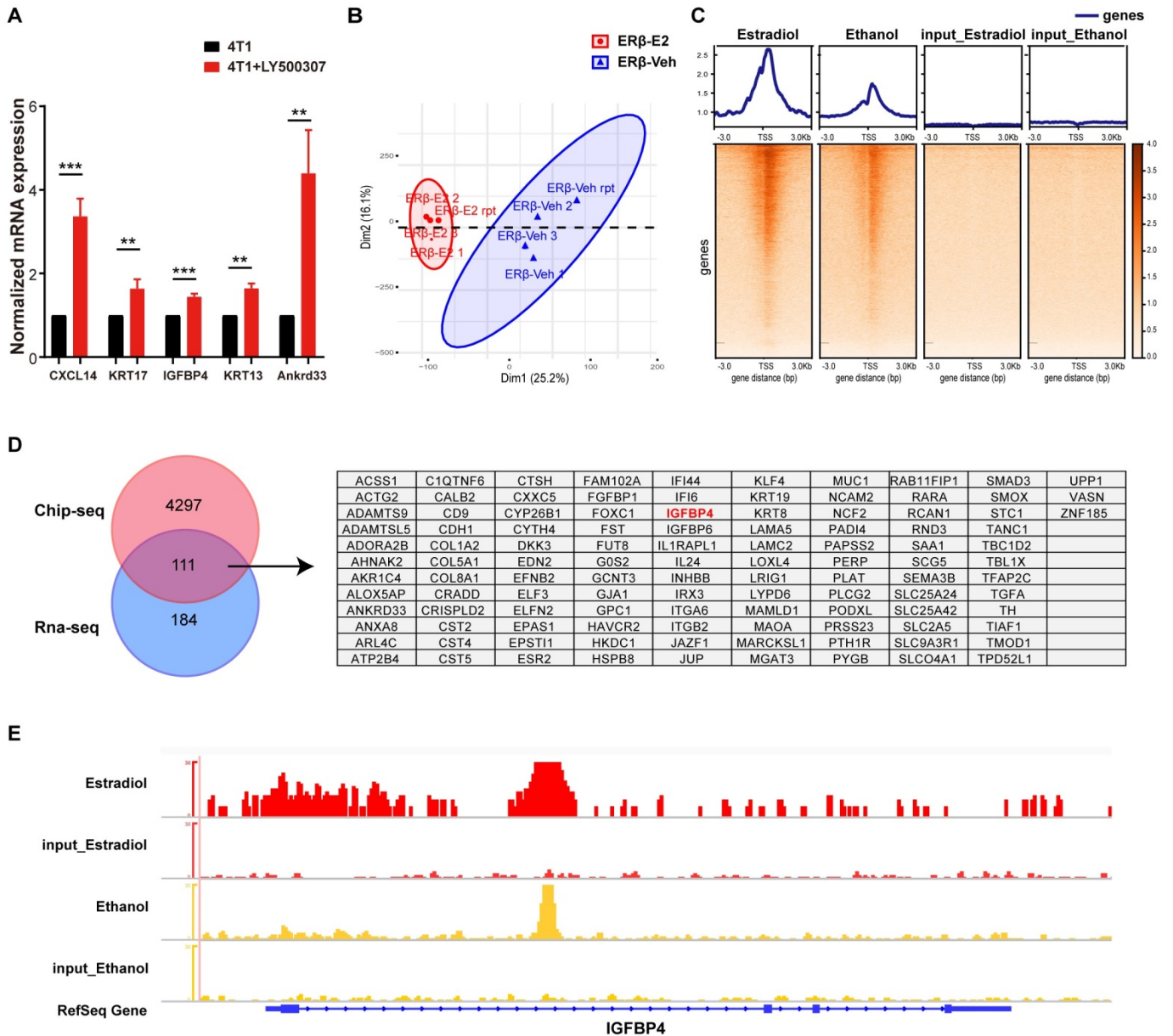
Shuang Huang, Nianxin Zhou, Linjie Zhao, Ryan C. Gimple, Young Ha Ahn, Peidong Zhang, Wei Wang, Bin Shao, Jingyun Yang, Qian Zhang, Sai Zhao, Xuehan Jiang, Zhiwei Chen, Yangfan Zeng, Hongbo Hu, Jan-Åke Gustafsson, and Shengtao Zhou

Supplementary Information

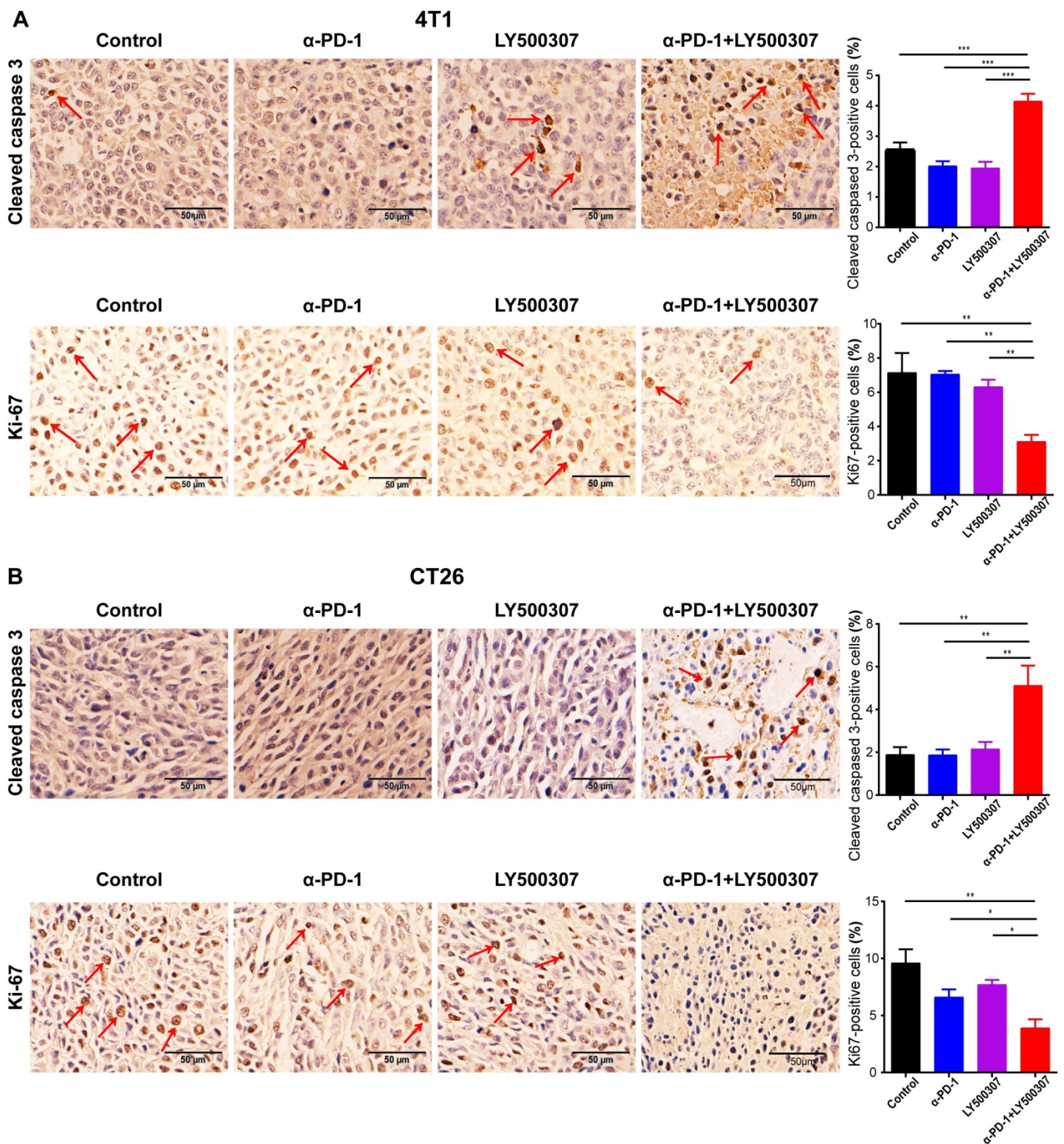
Pharmacological activation of estrogen receptor beta overcomes tumor resistance to immune checkpoint blockade therapy

Shuang Huang, Nianxin Zhou, Linjie Zhao, Ryan C. Gimple, Young Ha Ahn, Peidong Zhang, Wei Wang, Bin Shao, Jingyun Yang, Qian Zhang, Sai Zhao, Xuehan Jiang, Zhiwei Chen, Yangfan Zeng, Hongbo Hu, Jan-Åke Gustafsson, Shengtao Zhou

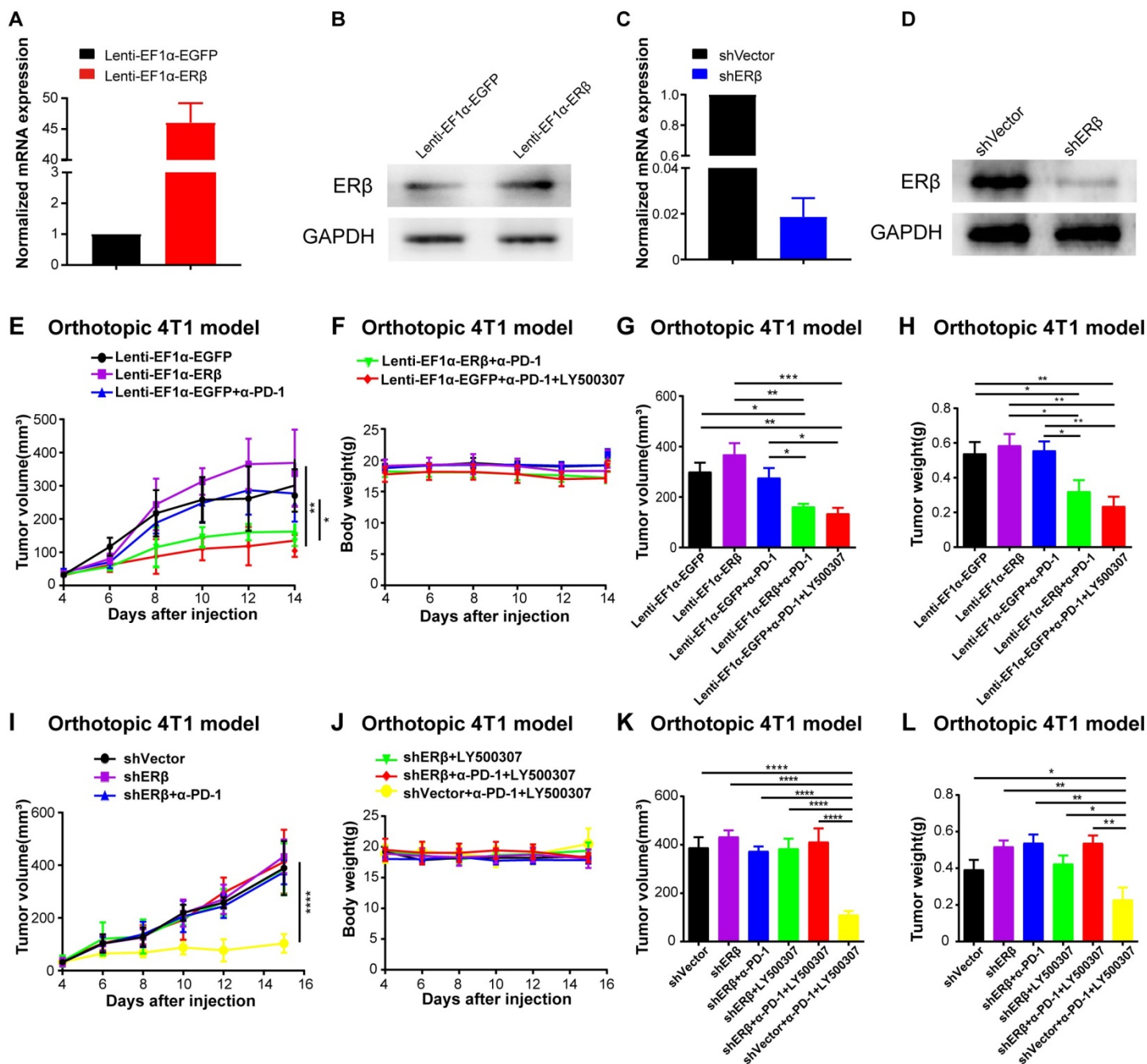
Supplementary Figures



Supplementary Figure 1(Related to Figure 1): The specificity of LY500307 for ERβ activation. (A) mRNA expression of known ERβ target genes. (B) PCA analysis of ERβ Chip sequencing data. (C) Heatmap of the differential ERβ-binding regions on DNA. (D) Venn diagram of ERβ Chip sequencing data and RNA sequencing data after ERβ activation shows that there are 111 *bona fide* ERβ targets. (E) Peak view of IGFBP4 as a representative ERβ-target gene. Data are shown as mean ±SEM. *, $P < 0.05$; **, $P < 0.01$; ***, $P < 0.001$.

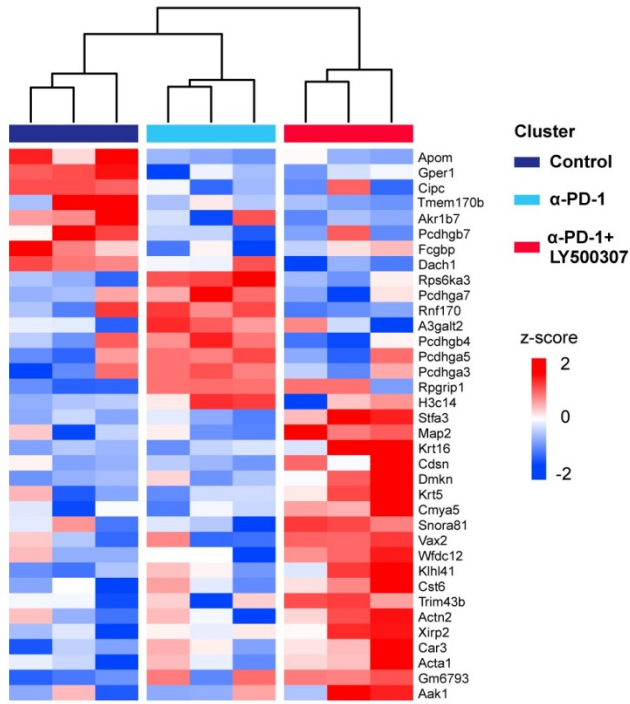
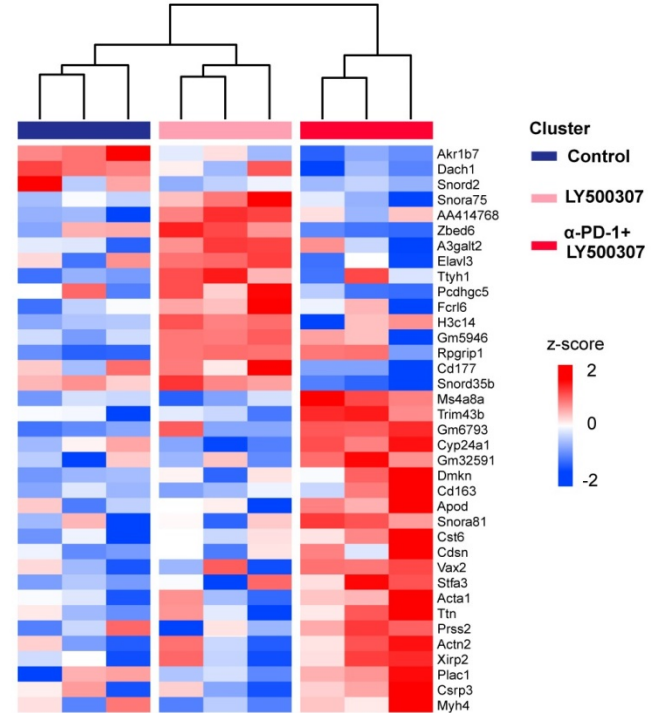


Supplementary Figure 2(Related to Figure 1): ER β activation induces apoptosis and proliferation arrest in ICB-resistant tumors. (A) Immunohistochemistry analysis of cleaved caspase 3 and Ki-67 in different treatment groups of 4T1 models (n=3 for each group). (B) Immunohistochemistry analysis of cleaved caspase 3 and Ki-67 in different treatment groups of CT26 models (n=3 for each group). Data are shown as mean \pm SEM; One-way ANOVA, *, $P < 0.05$; **, $P < 0.01$; ***, $P < 0.001$.

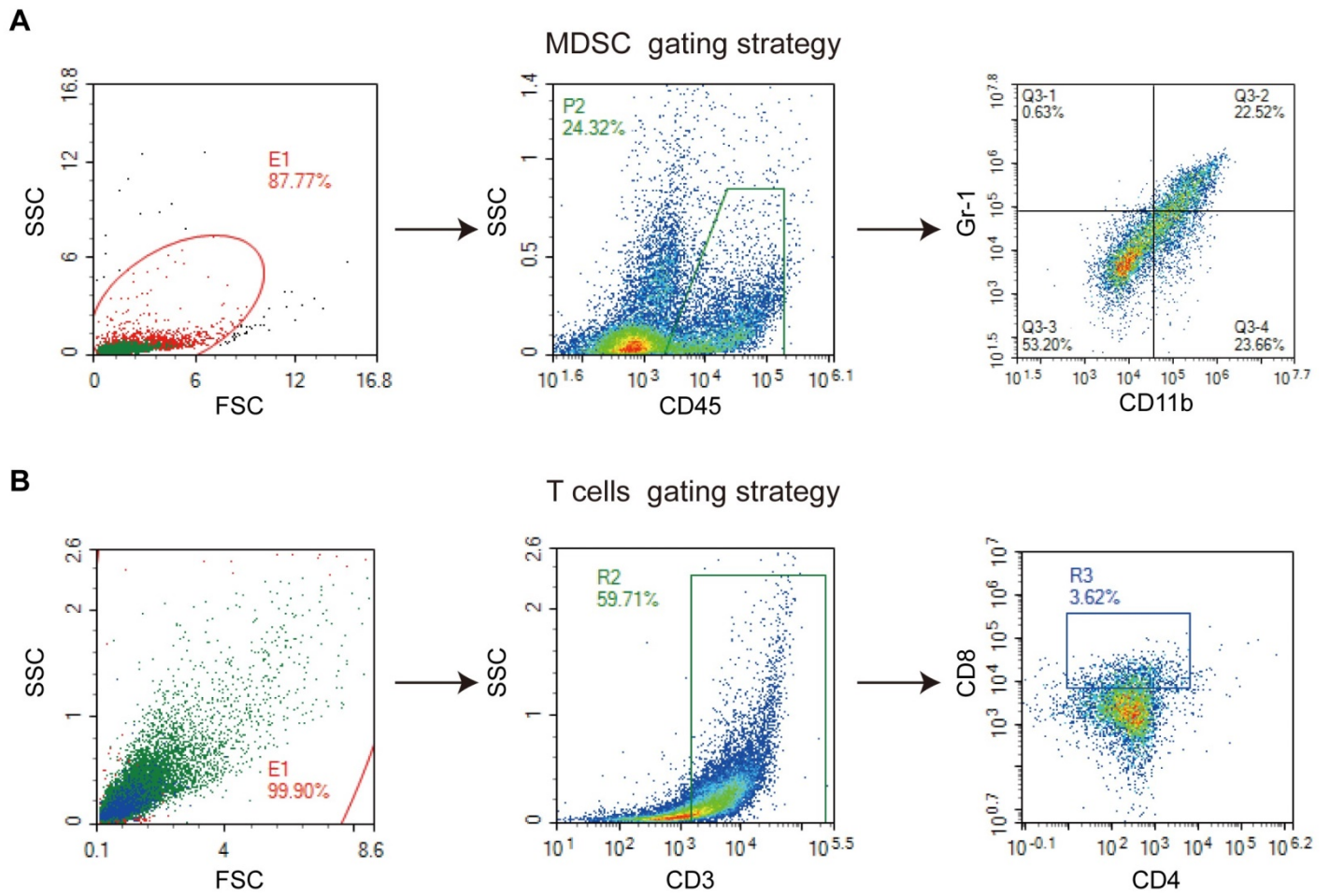


Supplementary Figure 3(Related to Figure 1): Genetic modulation of ERβ expression affects ICB therapy response. (A) Normalized mRNA expression of ERβ in ERβ-overexpressing 4T1 cells and control cells. (B) Protein level of ERβ in ERβ-overexpressing 4T1 cells and control cells. (C) Normalized mRNA expression of ERβ in ERβ-knockdown 4T1 cells and control cells. (D) Protein level of ERβ in ERβ-knockdown 4T1 cells and control cells. (E) BALB/c mice were orthotopically injected with each subset of 4T1 cells and each treatment was given at the indicated time. Growth kinetics was recorded at indicated time(n=5 for each group). (F) The body weight of orthotopic 4T1 murine model in each group at indicated time points

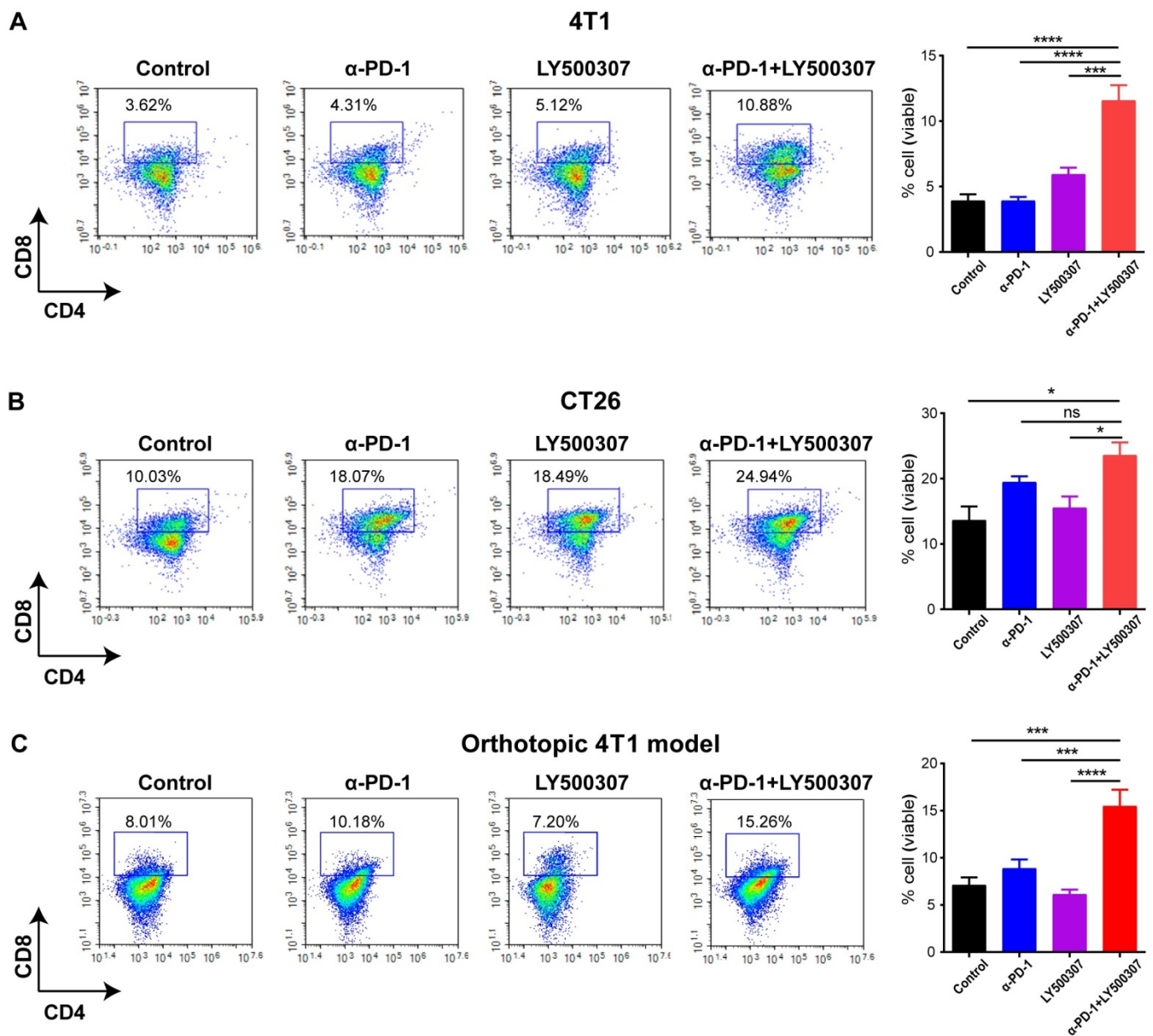
(n=5 for each group). (G) The tumor volume of orthotopic 4T1 murine model in each group at 14th day after tumor injection (n=5 for each group). (H) The tumor weight of orthotopic 4T1 murine model in each group at 14th day after tumor injection (n=5 for each group). (I) BALB/c mice were orthotopically injected with each subset of 4T1 cells and each treatment was given at the indicated time. Growth kinetics was recorded at indicated time (n=5-6 for each group). (J) The body weight of orthotopic 4T1 murine model in each group at indicated time points (n=5-6 for each group). (K) The tumor volume of orthotopic 4T1 murine model in each group at 15th day after tumor injection (n=5-6 for each group). (L) The tumor weight of orthotopic 4T1 murine model in each group at 15th day after tumor injection (n=5-6 for each group). Data are shown as mean±SEM; One-way ANOVA, *, $P < 0.05$; **, $P < 0.01$; ***, $P < 0.001$; ****, $P < 0.0001$.

A**B**

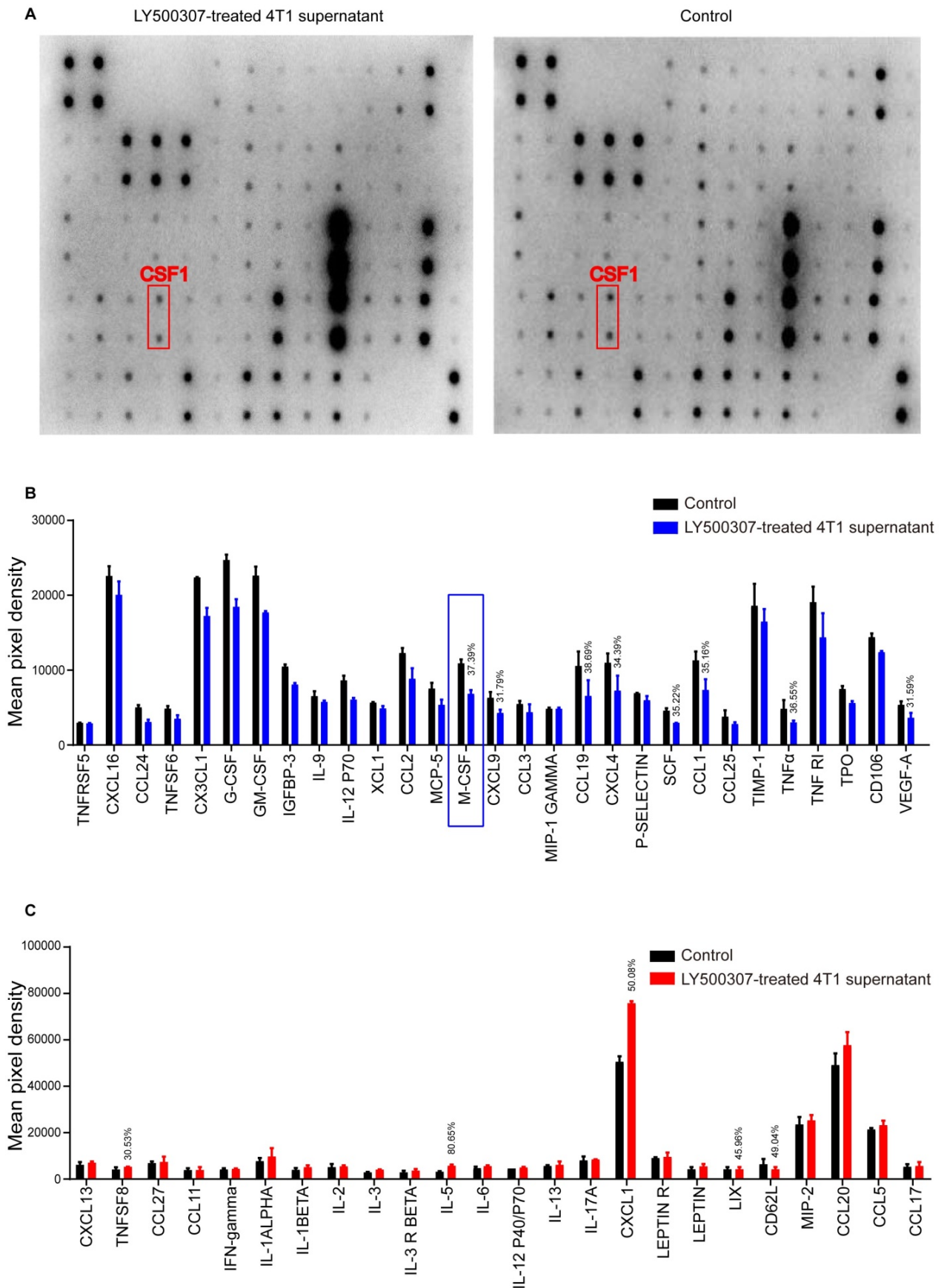
Supplementary Figure 4(Related to Figure 2): Heatmap of significantly altered genes between the combination treatment group and either drug as monotherapy groups.



Supplementary Figure 5(Related to Figure 2): Gating strategy for the flow cytometry analysis of MDSCs and T cells. (A) The gating strategy for the identification of tumor-bearing mouse MDSC subsets. (B)The gating strategy for the identification of tumor-bearing mouse CD8⁺ T cell subsets.



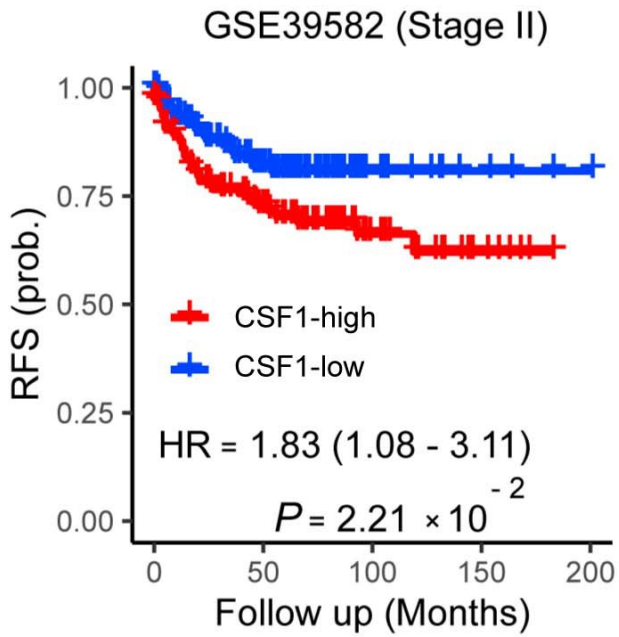
Supplementary Figure 6(Related to Figure 2): ER β activation reduces MDSC chemotaxis and enhances CD8⁺ T cells infiltration. (A) Flow cytometry analysis of CD8⁺ T cells in the tumor microenvironment of different treatment groups of 4T1 mouse model (n=3-4 for each group). (B) Flow cytometry analysis of CD8⁺ T cells in the tumor microenvironment of different treatment groups of CT26 mouse model (n=3 for each group). (C) Flow cytometry analysis of CD8⁺ T cells in the tumor microenvironment of different treatment groups of orthotopic 4T1 mouse model(n=5 for each group). Data are shown as mean \pm SEM; One-way ANOVA, *, $P < 0.05$; **, $P < 0.01$; *, $P < 0.001$; ****, $P < 0.0001$.**



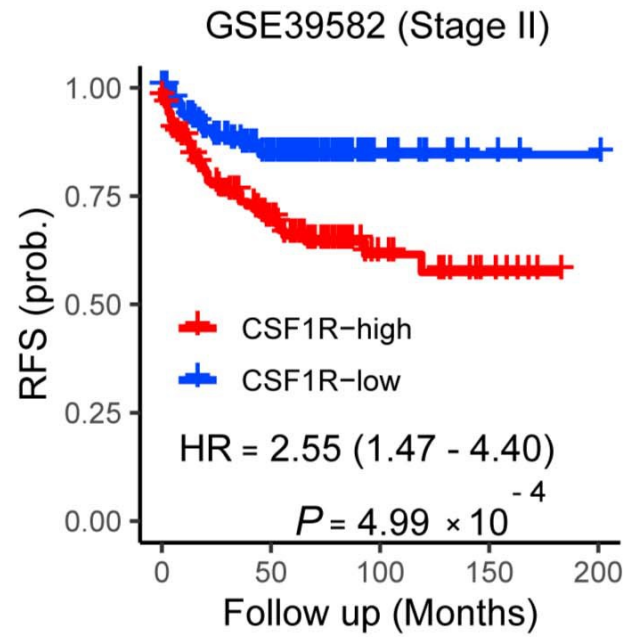
Supplementary Figure 7(Related to Figure 4): Raybio cytokine array analysis of 4T1 cells treated with LY500307. (A) Cytokine antibody array profiling of cytokine secretions in the LY500307-treated 4T1 conditioned media or control 4T1 conditioned media. (B) The mean pixel density shows the decreased secreted cytokines in 4T1

conditioned media treated with LY500307 compared with control and secreted cytokines reduced over 30% are labeled. (C)The mean pixel density shows the increased secreted cytokines in 4T1 conditioned media treated with LY500307 compared with control and secreted cytokines increased over 30% are labeled.

A



B



Supplementary Figure 8 (Related to Figure 6): CSF1/CSF1R axis informs prognosis in cancer patients. (A) Correlation of CSF1 expression with RFS in CRC patients of GSE39582 dataset. (B) Correlation of CSF1R expression with RFS in CRC patients of GSE39582 dataset.

Transparent Methods

Cell culture, reagent information and lentiviral transfection

The mouse breast cancer cell line 4T1 and the mouse colorectal cancer cell line CT26 were obtained from the American Type Culture Collection (ATCC). Cells were propagated in Roswell Park Memorial Institute (RPMI) 1640 medium containing 10% fetal bovine serum (FBS; Gibco, Auckland, N.Z.) and 1% antibiotics (penicillin and streptomycin) in 5% CO₂ at 37 °C. The lentivirus systems for both ERβ knockdown and overexpression were purchased from the Obio technology(Shanghai, China). To explore the function of ERβ overexpression in 4T1 mouse model, we used the pSLenti-EF1α-EGFP-P2A-Puro-CMV-Esr2-3Flag lentivirus and pRLenti-EF1α-EGFP-P2A-Puro-CMV-MCS-3Flag lentivirus. To explore the function of ERβ knockdown in 4T1 mouse model, we used the pLKD-CMV-EGFP-2A-Puro-U6-shRNA(control) and pLKD-CMV-EGFP-2A-Puro-U6-shRNA (Esr2). Virus were treated with 10 μg/mL polybrene prior to infecting cells, and stable cell lines were selected out in 1 μg/mL puromycin for 48 hrs. The mRNA and protein levels of ERβ in each cell line were determined by qPCR and immunoblotting, respectively. The primary antibody of ERβ was purchased from Abcam (ab3577).

Animal treatment

Female BALB/c (Six- to eight-week-old) mice were purchased from Vital River (Beijing, China). These mice were housed in a specific-pathogen-free (SPF) environment with a consistent room temperature and humidity. All animal experiments were approved by the Institutional Animal Care and Use Committee and Ethics Committee of Sichuan University. Briefly, subcutaneously injection of 100uL tumor cell suspension containing 1×10^6 4T1 cells or CT26 tumor cell in each BALB/c mouse or orthotopic injection of 4T1 cells into the mammary fat pad of BALB/c mouse were performed, respectively. The mice were orally administered with vehicle or 0.04mg LY500307 (KareBay Biochem) per day since the third day after inoculation of tumors. PD-1 antibody (BE0146, Bioxcell) was administered 200ug i.p.

every two days. Gr-1 antibody (clone RB6-8C5, Bioxcell) was administered 200ug i.p. every two days. CSF1R antibody (clone AFS98 ,Bioxcell) was administered 300ug i.p. every two days. Body weight and tumor volume were assessed every two days. When all animals were euthanized, the tumor weight and volume were measured.

RNA sequencing and bioinformatics analysis

The bulk tumor tissues of 4T1 models in each treatment group were collected at indicated time and total RNA was isolated using RNeasy Mini Kit (Qiagen) according to the manufacturer's instructions. The purity of prepared RNA was determined using an Agilent 2100 BioAnalyzer. Illumina TruSeq RNA sample preparation was performed following the manufacturer's protocol, and the samples were run on an Illumina HiSeq2000. The combined raw reads were aligned to University of California, Santa Cruz Genome Browser mm9 mouse sequence assembly, and the genes were annotated by Tophat. Genes were annotated and quantified by high-throughput sequencing–DESeq pipeline. Differential expression analysis was performed by DESeq and significant genes with at least 1.5-fold change with $P < 0.05$ were chosen for visualization on heatmaps. Unsupervised clustering of each RNA-seq sample with PCA analysis was performed using R package FactoMineR. Gene ontology (GO) enrichment analysis was performed using R package clusterprofiler. Chip sequencing analysis of ER β target genes for the publicly available dataset GSE108979 was performed using methods described elsewhere (Yu et al., 2013).

Flow cytometry

For detection of MDSCs and T cells *in vivo*, the mouse tumor was minced and digested with 1 mg/mL collagenase I in 37 °C for 2 h. After erythrocyte lysis, the cells were washed with PBS and stained with the primary antibodies (BD Bioscience and BioLegend), including anti-CD45, anti-CD11b, anti-Gr1, anti-CD3, anti-CD4, and anti-CD8 mAb. Cells were stained with primary antibodies and then analyzed with flow cytometry (NovoCyte; ACEA Biosciences).

ELISA assay

4T1 (3×10^5 cells per well) or CT26 cells (3×10^5 cells per well) were seeded in a 10-mL plate for 12 h and treated with medium containing LY500307 (5 μ M) or vehicle. After treatment for 48 h, the cell supernatant was collected, centrifuged and filtered with a 0.22 μ m strainer. The cell supernatants were obtained to measure the production of murine CSF1 using Quantikine ELISA kit (R&D System MMC00) according to the manufacturer's instruction.

qPCR

The mRNA level of each gene was measured via qPCR as described previously (Zhao et al., 2017). Briefly, total RNAs were isolated using TRIzol reagent(Invitrogen) according to the manufacturer's instructions. First strand cDNA was reversely transcribed from 1 μ g of total RNA in a final volume of 20 μ g using RTase and random hexamers from ExScript reagent kit(TAKARA, Dalian, China) according to the manufacturer's instructions. The sequences of the primers used for all qPCR assays are as follows: CSF1 forward: ATGAGCAGGAGTATTGCCAAGG; CSF1 reverse: TCCATTCCCAATCATGTGGCTA; Esr2 forward: CTGTGCCTCTTCTCACAAGGA; Esr2 reverse: TGCTCCAAGGGTAGGATGGAC; iNOS forward: GTTCTCAGCCCAACAATACAAGA; iNOS reverse: GTGGACGGGTTCGATGTCAC; IDO forward: GCTTTGCTCTACCACATCCAC; IDO reverse: CAGGCGCTGTAACTGTGT; CD80 forward: ACCCCAACATAACTGAGTCT; CD80 reverse: TTCCAACCAAGAGAAGCGAGG; TLR4 forward: ATGGCATGGCTTACACCACC; TLR4 reverse: GAGGCCAATTTTGTCTCCACA; CD86 forward: TGTTTCCGTGGAGACGCAAG; CD86 reverse: TTGAGCCTTTGTAAATGGGCA; β -actin forward: ACCGCTCGTTGCCAATAGTGATGA; β -actin reverse: TGAGAGGGAAATCGTGCGTGACAT.

Isolation of mouse MDSCs and ex vivo MDSC migration assay

Mouse MDSCs were prepared from isolated spleen as previously described (Alizadeh et al., 2014) with minor modifications. Briefly, 14 days post-tumor injection, spleens were harvested, dissociated and red blood cells were lysed in lysis buffer (BD biosciences). MDSCs were purified using a mouse MDSC isolation kit according to the manufacturer's instructions (Miltenyi Biotec 130-094-538). Transwell chamber migration assay was performed to assess the *ex vivo* MDSCs migratory potential as previously described (Zhao et al., 2018; Zhao et al., 2017) with minor modifications. Briefly, MDSCs in 200 μ L of serum-free medium or CSF1R antibody plus serum-free medium were added in the top chamber, and then 500 μ L of medium with 4T1 supernatant, LY500307 plus 4T1 supernatant, LY500307 pre-treated 4T1 supernatant was added to the bottom chamber. MDSCs were allowed to migrate for 48 h. Non-migrated cells in the top chamber were removed. The migrated cells were fixed in 4% paraformaldehyde and stained with 0.5% crystal violet. Migrated cells were counted and photographed under a light microscope.

Immunohistochemistry and immunofluorescent analysis

TNBC and colorectal cancer patient specimens used for immunohistochemistry analysis were collected from West China Hospital, Sichuan University. All of the samples were examined by experienced pathologists who confirmed the diagnosis of disease samples. This study was approved by the Institutional Ethics Committee of Sichuan University. Informed consents were obtained from all patients prior to analysis. Immunohistochemistry staining was described previously (Zhao et al., 2019; Zhou et al., 2012). The antibodies used for immunohistochemistry analysis include: Gr-1(R&D Systems), CSF1 (Abcam, ab233387), CSF1R (Abcam, ab215441), cleaved caspase-3(Cell Signaling Technology, 9661), and Ki-67(Abcam, ab15580). Immunofluorescent analysis was conducted as described previously (Zhou et al., 2012). The information of primary antibodies is as follows: CSF1R (Abcam,

ab215441) and Gr-1((Biolegend, 108401). DAPI was used for nuclei staining. Stained sections were viewed and photographed through a fluorescence microscope.

Raybio cytokine array

For cytokine antibody array, the conditioned media for LY500307-treated 4T1 and control were collected and used directly without further dilution. Semiquantitative detection of 62 mouse proteins in the conditioned media was performed using RayBio® C-Series Mouse Cytokine Antibody Array C3 (RayBiotech, Inc, #AAM-CYT-3-2) according to the manufacturer's instructions. Detection of dots was performed with the ChemiDoc MP Imaging Systems (Bio-Rad).

Public dataset survival analysis

We used the publicly available GSE39582 dataset (Marisa et al., 2013) comprising a total of 260 colorectal patients for survival analysis. Gene expression data together with clinical profiles were downloaded from Gene Expression Omnibus (GEO) directly in their processed form using R package GEOquery (Davis and Meltzer, 2007) (version 1.0.7).

Statistical analysis

For studies comparing differences between two groups, unpaired Student's *t* tests were used. For studies comparing more than two groups, one way ANOVA *post hoc* Student-Newman-Keuls test was applied. Differences were considered significant when $P < 0.05$. Data are presented as mean \pm SEM.

Supplemental references

Alizadeh, D., Trad, M., Hanke, N.T., Larmonier, C.B., Janikashvili, N., Bonnotte, B., Katsanis, E., and Larmonier, N. (2014). Doxorubicin eliminates myeloid-derived suppressor cells and enhances the efficacy of adoptive T-cell transfer in breast cancer. *Cancer Res.* *74*, 104-118.

Davis, S., and Meltzer, P.S. (2007). GEOquery: a bridge between the Gene Expression Omnibus (GEO) and BioConductor. *Bioinformatics* *23*, 1846-1847.

Marisa, L., de Reynies, A., Duval, A., Selves, J., Gaub, M.P., Vescovo, L., Etienne-Grimaldi, M.C., Schiappa, R., Guenot, D., Ayadi, M., *et al.* (2013). Gene expression classification of colon cancer into molecular subtypes: characterization, validation, and prognostic value. *PLoS Med.* *10*, e1001453.

Yu, Y., Chen, Y., Kim, B., Wang, H., Zhao, C., He, X., Liu, L., Liu, W., Wu, L.M., Mao, M., *et al.* (2013). Olig2 targets chromatin remodelers to enhancers to initiate oligodendrocyte differentiation. *Cell* *152*, 248-261.

Zhao, L., Huang, S., Mei, S., Yang, Z., Xu, L., Zhou, N., Yang, Q., Shen, Q., Wang, W., Le, X., *et al.* (2018). Pharmacological activation of estrogen receptor beta augments innate immunity to suppress cancer metastasis. *Proc. Natl. Acad. Sci. U. S. A.* *115*, E3673-E3681.

Zhao, L., Ji, G., Le, X., Wang, C., Xu, L., Feng, M., Zhang, Y., Yang, H., Xuan, Y., Yang, Y., *et al.* (2017). Long noncoding RNA LINC00092 acts in cancer-associated fibroblasts to drive glycolysis and progression of ovarian cancer. *Cancer Res.* *77*, 1369-1382.

Zhao, L., Wang, W., Xu, L., Yi, T., Zhao, X., Wei, Y., Vermeulen, L., Goel, A., Zhou, S., and Wang, X. (2019). Integrative network biology analysis identifies miR-508-3p as the determinant for the mesenchymal identity and a strong prognostic biomarker of ovarian cancer. *Oncogene* *38*, 2305-2319.

Zhou, S., Yi, T., Liu, R., Bian, C., Qi, X., He, X., Wang, K., Li, J., Zhao, X., Huang, C., *et al.* (2012). Proteomics identification of annexin A2 as a key mediator in the metastasis and proangiogenesis of endometrial cells in human adenomyosis. *Mol. Cell. Proteomics* *11*, M112 017988.